

# Matrix Pencil-Based DoA Estimation for Hybrid Receivers in Snapshot-Limited Scenarios

Mona Mostafa, Ramy H. Gohary, Amr El-Keyi, and Yahia A. Eldemerdash Ahmed

**Abstract**— The goal of this paper is to estimate the directions of arrival (DoAs) for hybrid analog/digital (HAD) receivers when the number of snapshots is too small for statistical averaging to be reliable. This goal is achieved in fully-digital receivers by employing the matrix pencil method (MPM). Unfortunately, the MPM cannot be directly applied in HAD receivers because of the entanglement induced by the underlying analog combiners on the output signals. Furthermore, these analog combiners project the received signal onto a low-dimensional space, jeopardizing the reception of signals arriving from particular DoA ranges. To circumvent these difficulties, we propose two approaches to enable the MPM to extract the DoAs in HAD receivers. The two approaches avoid severe attenuation induced by low-dimensional projection by cycling over an exhaustive set of analog combiners, collectively spanning the entire space. The first approach can be applied to both fully-connected (FC) and partially-connected (PC) HADs and relies on the availability of periodic, potentially unknown, signals to disentangle the output of the HAD receiver. The second approach applies to PC-HADs only, and eliminates contingency on periodic signals by exploiting the underlying block diagonal structure. The superiority of the proposed approaches is demonstrated via numerical simulations and comparisons with the Cramér-Rao lower bound.

## I. INTRODUCTION

Direction of arrival (DoA) estimation is essential for both military and civilian wireless communications [1], [2], including secure data transmission, aircraft, and maritime tracking, Internet of Things (IoT) applications [3], [4], unmanned aerial vehicles (UAVs) communications [5], and emerging, 5G+, cellular systems [6]. DoA estimation techniques have traditionally relied on collecting a large number of snapshots. However, when the wireless channel undergoes rapid changes, collecting a large number of snapshots becomes practically infeasible, especially under stringent processing time constraints [7]. This calls for techniques that enable accurate DoA estimation using a small number of snapshots to be developed.

In addition to having access to a large number of snapshots, accurate DoA estimation requires the receiver to be equipped with a large number of antennas, to improve its spatial resolution, i.e., its ability to distinguish between neighbouring DoAs [2]. Having a large number of antenna elements comes at a heavy price: increased hardware cost and complexity, and power consumption of the radio frequency (RF) chains needed for down-conversion and digitization [8]–[10]. These challenges are exacerbated in classical fully-digital (FD) receivers, wherein each antenna is connected to a dedicated RF chain. One approach to overcome this limitation is to

replace FD receivers with their analog counterparts [11], [12]. Unfortunately, the accuracy of the estimates generated by fully analog receivers is significantly less than that generated by their FD counterparts. This is because FD receivers process the amplitudes and phases of the received signals, whereas fully analog receivers process their phases only [9], [13]. A versatile class of architectures that enable trading hardware-related difficulties for estimation accuracy is that comprising hybrid analog/digital (HAD) receivers [13]–[16].

In HAD receivers, the antenna processing unit is divided into an analog combiner, implemented using analog phase shifters, and a digital combiner connected to a relatively small number of RF chains [15]. By choosing the number of antennas connected to each RF chain, HAD receivers offer a trade-off between estimation accuracy and hardware complexity [17]. Among existing HAD receivers, are the fully-connected (FC) [18] and partially-connected (PC) [19], [20] ones. In FC-HAD, each RF chain is connected to all the antennas through phase shifters, whereas in PC-HAD, only a subset of antennas is connected to each RF chain.

Several DoA estimation techniques have been developed for classical FD receivers, e.g., [21]–[32]. Among these techniques are the Bartlett and the minimum variance distortionless response (MVDR) ones [21], [22], which involve a linear search over all possible DoAs. Another class of techniques relies on received signal statistics. For instance, the multiple signal classification (MUSIC) and the minimum norm (NM) techniques rely on estimating the covariance matrix and subsequently restricting the linear search to the subspace dominantly occupied by the received signal [23]–[25]. Related techniques that incur reduced computational complexity include root-MUSIC [26] and the estimation of signal parameters via rotational invariance technique (ESPRIT) [27]. Apart from Bartlett and MVDR, which are computationally intensive, all aforementioned algorithms depend on the true covariance matrix, which is often unavailable, especially when the number of received snapshots is limited. A technique that alleviates the aforementioned challenges relies on the so-called matrix pencil method (MPM) [28]–[32]. This method relies on the received signal structure rather than statistics, enabling DoA estimation of multiple sources even with limited snapshots.

Some of the classical, statistics-based, DoA estimation techniques originally developed for FD receivers have been extended to HAD ones. For instance, in [33], root-MUSIC is applied in PC-HAD receivers with single-phase analog combiners. This approach enables reliable estimation within a particular spatial sector but unreliable estimates outside it. This drawback is addressed by other methods through successive

The first two authors are with the Department of Systems and Computer Engineering, Carleton University, Ottawa, ON K1S5B6, Canada. The last two authors are with Ericsson Canada Inc., Mississauga, ON, Canada.

tuning of the analog combiner to angles that are drawn from either a random [8] or a predefined [34]–[36] set. Despite their effectiveness, these techniques rely on statistical averaging, which require a large number of snapshots to obtain accurate estimates of the underlying covariance matrices [8], [34], [35] and signal power [33], [36]. Obtaining such a number of snapshots incurs potentially intolerable delay and may not be feasible under high mobility conditions. Another class of DoA estimation techniques uses compressed sensing [14], [15], [37]. Such techniques, are computationally demanding, but are generally effective when the underlying channel is sparse, as in millimeter-wave communications. Finally, DoA estimation techniques that rely on deep learning have been proposed in [38]–[40]. Unfortunately, these techniques involve extensive training overhead and their performance is questionable when employed in environments not covered by the training phases.

In this paper, we consider DoA estimation in HAD receivers under stringent constraints on the number of snapshots available for the receiver. These constraints render statistical averaging unreliable, and techniques that rely on exploiting the structure embedded in the received signals, rather than their sample averages, must be sought. One technique to do so is the MPM. Unfortunately, this technique, although readily applicable in FD receivers [28], [30], [32] does not automatically lend itself to HAD receivers. In particular, we will show that HAD architectures tangle the signal at the receiver output, rendering the invocation of the MPM rather unwieldy. Furthermore, we will show that the analog combiner of the HAD receiver projects the received signal vector onto a hyperplane corresponding to a particular spatial sector. This projection causes the signals arriving from particular DoAs to be attenuated or even nullified. To address these challenges, we develop two new MPM-centered approaches.

In the first approach, the attenuation incurred by the analog combiner is mitigated by cycling over an exhaustive set of analog combiners that collectively span the entire space. Such analog combiners can be constructed from the Discrete Fourier Transform (DFT) matrix. The main idea of this approach is to exploit the fact that, in typical communications, the received signal comprises periodic, potentially unknown, deterministic components to assist the receiver in data recovery [41]. Such signals include training pilots or the preamble segment of the signal frame. We will show that access to such signals can be used to combine and disentangle the signals at the outputs of the analog combiners. Hence, this approach renders HAD receivers, either FC or PC, behave as if they were FD insofar as their output is amenable to DoA estimation via the MPM, and the attenuation incurred by individual analog combiners is alleviated. Despite its efficacy, the first approach relies on extracting periodicity embedded in the received signal frames. This requires recovery of the timing of the periodic segments, adding to the complexity and processing delay of the receiver.

In the second approach, we seek to eliminate the reliance on periodic signals characteristic of the first approach. To do so, we note that the entanglement of the received signals at the output of the analog combiner results from the non-identical phases of the columns used to construct the underlying matrices. To address this problem, we construct the

analog combiner using a single column from the DFT matrix. Doing so in FC-HAD results in rank-one analog combiners, causing the structure of their output to be degenerate for the MPM to be applicable. In contrast, the analog combiners in PC-HAD receivers possess a block-diagonal structure, which preserves the linear independence of the columns, even when they have identical phases. As such, these analog combiners result in their outputs to be disentangled and thereby amenable to the MPM. Similar to the first approach, to remedy the attenuation incurred by the analog combiner, we cycle over an exhaustive set of analog combiners. Phase ambiguity inherent in this approach can be resolved by reconfiguring the analog combiner based on the estimated DoAs and selecting the ones that maximize the received signal-to-noise ratio (SNR). As such, the second approach trades periodic signals needed by the first approach for an increased number of snapshots, which is required to resolve its inherent phase ambiguity.

Root-mean-square error (RMSE) simulations and the corresponding Cramér-Rao lower bound (CRLB) show the superiority of the proposed approaches over their existing counterparts.

The rest of the paper is organized as follows. The system model is presented in Section II. Section III states the problem formulation. The proposed approaches are presented in Section IV. Simulation results are provided in Section V, and Section VI concludes the paper.

Notations: Matrices and vectors are denoted by upper and boldface lower case letters, respectively. The transpose, left pseudo-inverse, and Hermitian are denoted by  $(\cdot)^T$ ,  $(\cdot)^\dagger$ , and  $(\cdot)^H$ , respectively. The  $M \times M$  identity matrix and the  $M \times 1$  all one column vector are denoted by  $\mathbf{I}_M$  and  $\mathbf{1}_M$ , respectively. The trace and eigenvalues of a matrix are denoted by  $\text{Tr}(\cdot)$ , and  $\nu(\cdot)$ , respectively. The Kronecker, Hadamard products and the direct sum are denoted  $\otimes$ ,  $\odot$  and  $\oplus$ , respectively.

## II. SYSTEM MODEL

We consider a uniform linear array (ULA) of  $M$  identical antennas. The objective is to estimate the DoAs,  $\{\theta_r\}_{r=1}^R$ , corresponding to far-field narrowband signals emitted by  $R$  distinct sources. The ULA steering vector corresponding to the  $r$ -th source,  $r = 1, \dots, R$ , are given by [8], [33], [34]:

$$\mathbf{a}_r = [1 \quad e^{j\mu_r} \quad \dots \quad e^{j(M-1)\mu_r}]^T, \quad (1a)$$

$$\mu_r = \frac{2\pi\Delta}{\lambda} \sin \theta_r, \quad (1b)$$

where  $\lambda$  is the wavelength,  $\Delta \leq \frac{\lambda}{2}$  is the antenna spacing, and  $\mu_r \in (-\pi, \pi]$  is the phase between adjacent antennas [21].

Let the steering vectors of all sources be contained in the matrix  $\mathbf{A} = [\mathbf{a}_1 \cdots \mathbf{a}_R] \in \mathbb{C}^{M \times R}$ . Let the  $R$  unknown baseband signals be denoted as  $\mathbf{s}(t) = [s_1(t) \cdots s_R(t)]^T$ . The received signals at the antenna array can be modelled as:

$$\mathbf{x}(t) = e^{j2\pi f_c t} \mathbf{A} \mathbf{s}(t) + \mathbf{z}(t), \quad (2)$$

where  $f_c$  is the carrier frequency and  $\mathbf{z}(t) \in \mathbb{C}^M$  is the zero-mean additive white Gaussian unit variance noise, i.e.,  $\sigma_z^2 = 1$ .

After down-conversion, the signal is sampled at  $T_s$  intervals and the  $k$ -th snapshot is given by  $\mathbf{x}_k \in \mathbb{C}^M$ , where

$$\mathbf{x}_k = \mathbf{A} \mathbf{s}(t) + \mathbf{z}(t) \Big|_{t=kT_s}, \quad k = 1, \dots, \tilde{K}, \quad (3)$$

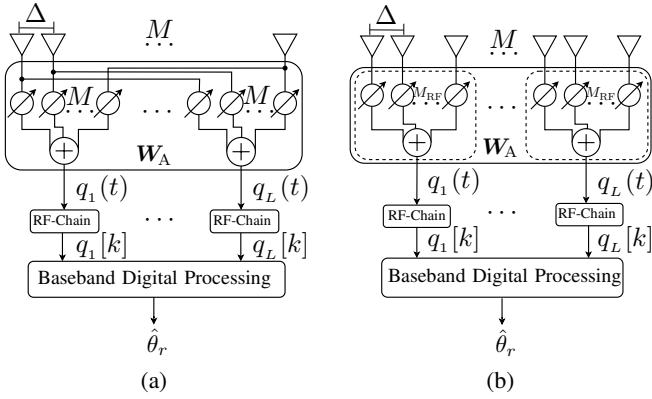


Figure 1: Block diagram of (a) FC-HAD, (b) PC-HAD.

where  $\tilde{K} = NK$  represents the number of snapshots contained in  $N$  length- $K$  segments. In matrix notation, we can write (3):

$$\mathbf{X}_n = \mathbf{A}\mathbf{S}_n + \mathbf{Z}_n, \quad (4)$$

where the  $mk$ -th entry of  $\mathbf{X}_n$  and  $\mathbf{Z}_n \in \mathbb{C}^{M \times K}$  represents the  $k$ -th sample of the received signal and noise at the  $m$ -th antenna of the  $n$ -th segment of snapshots, respectively,  $m = 1, \dots, M$ . The  $rk$ -th entry of  $\mathbf{S}_n \in \mathbb{C}^{R \times K}$  represents the  $k$ -th sample of signal emitted by the  $r$ -th source,  $r = 1, \dots, R$ ,  $k = 1, \dots, K$ . For uncorrelated sources,

$$\Phi = \frac{1}{K} \mathbb{E}\{\mathbf{S}_n \mathbf{S}_n^H\} = \text{diag}(P_1, \dots, P_R), \quad (5)$$

where  $\{P_r\}_{r=1}^R$  represent the average power of the  $R$  sources.

We now review FC-HAD and PC-HAD receivers [17]–[19].

#### A. The HAD Receiver

In HAD receivers, the  $n$ -th segment of snapshots from the  $M$  antennas in (2) are fed to the analog combiner,  $\mathbf{W}_{A,n} \in \mathbb{C}^{M \times L}$ , which phase-shifts and combines the outputs into  $L < M$  streams, cf. Figure 1. Each of the  $L$  streams is composed of a subarray of  $M_{\text{RF}}$  antennas connected to one RF chain for down-conversion and digitization. The output of  $\mathbf{W}_{A,n}$  is:

$$\mathbf{q}(t) = \mathbf{W}_{A,n}^H \mathbf{x}(t). \quad (6)$$

A key limitation of the analog combiner is not to contain active elements. Incorporating such elements is both costly and impractical for systems with a large number of antennas. Hence, the analog combiner is restricted to phase-shifting the output of each antenna without storing it or altering its power [14]. Down-converting and sampling  $\mathbf{q}(t)$  yields:

$$\mathbf{q}_k = e^{-j2\pi f_c t} \mathbf{q}(t) \Big|_{t=kT_s}, \quad k = 1, \dots, K. \quad (7)$$

Collecting  $\{\mathbf{q}_k\}_{k=1}^K$  in the matrix  $\mathbf{Q}_n \in \mathbb{C}^{L \times K}$ , we write (7):

$$\mathbf{Q}_n = \mathbf{W}_{A,n}^H \mathbf{A}\mathbf{S}_n + \mathbf{W}_{A,n}^H \mathbf{Z}_n, \quad (8)$$

where  $\mathbf{Q}_n \in \mathbb{C}^{L \times K}$  is the output of  $\mathbf{W}_{A,n}$ , which is then fed to the baseband digital DoA estimator.

Among existing HAD receivers are the FC-HAD and PC-HAD ones. In both receivers, all non-zero entries of  $\mathbf{W}_A^1$  are unit-modulus in the form  $e^{j\phi}$ ,  $\phi \in (-\pi, \pi]$ . For FC-HAD and PC-HAD,  $\mathbf{W}_A$  is denoted as  $\mathbf{W}_{\text{AFC}}$  and  $\mathbf{W}_{\text{APC}}$ , respectively.

<sup>1</sup>The subscript,  $n$ , is dropped in discussions pertaining to all combiners.

1) *The FC-HAD Receiver:* In FC-HAD, each RF chain is connected to all antenna elements via  $ML$  analog phase shifters, cf. Figure 1a. As shown in this figure, the output of each antenna is split across the  $L$  phase shifters and RF chains. Hence,  $\mathbf{W}_{\text{AFC}}$  can be expressed as:

$$\mathbf{W}_{\text{AFC}} = \frac{1}{\sqrt{L}} [\mathbf{w}_{\text{AFC},1} \ \dots \ \mathbf{w}_{\text{AFC},L}], \quad (9)$$

where  $\mathbf{w}_{\text{AFC},\ell} \in \mathbb{C}^M$  contains the  $M_{\text{RF}} = M$  phase shifts of the  $\ell$ -th subarray,  $\ell = 1, \dots, L$ . The scalar multiplier, i.e.,  $\frac{1}{\sqrt{L}}$ , accounts for the power splitting at the antenna outputs.

2) *The PC-HAD Receiver:* In PC-HAD, the antenna outputs are not split across multiple phase shifters. Instead, each antenna is connected to one phase shifter before combining into one RF chain, cf. Figure 1b. In other words, in this receiver, the  $M$  receive antennas are partitioned into  $L$  identical subarrays, whereby each subarray contains  $M_{\text{RF}} = M/L$  antennas. For convenience, we assume that  $M$  is a multiple integer of  $L$ . As such, PC-HAD receivers use  $M$  analog phase shifters, in contrast with the  $ML$  ones used in FC-HAD. Since in PC-HADs, the  $L$  subarrays are connected to distinct antenna elements,  $\mathbf{W}_{\text{APC}}$  features a block diagonal structure, wherein the  $\ell$ -th diagonal block is the vector  $\mathbf{w}_{\text{APC},\ell} \in \mathbb{C}^{M_{\text{RF}}}$ , representing the  $M_{\text{RF}}$  phase shifters of  $\ell$ -th subarray. Hence,

$$\mathbf{W}_{\text{APC}} = \bigoplus_{\ell=1}^L \mathbf{w}_{\text{APC},\ell}, \quad (10)$$

where, similar to their FC counterparts, the entries of  $\mathbf{w}_{\text{APC},\ell} \in \mathbb{C}^{M_{\text{RF}}}$  are in the form  $e^{j\phi}$ ,  $\ell = 1, \dots, L$ .

Although versatile and effective, the performance of HAD receivers is constrained by the unit-modulus analog phase shifters and suffers from a notable weakness due to the reduced dimensionality incurred by the analog combiner. In particular, from (6), the analog combiner,  $\mathbf{W}_A \in \mathbb{C}^{L \times M}$ , projects the received signals onto  $L < M$  dimensions. This projection results in severe attenuation or even nullification of the signals received from particular DoAs. Two approaches for addressing this weakness will be developed in Section IV.

### III. PROBLEM FORMULATION

In this section, we consider the practical scenario in which the number of snapshots available to the receiver is too small for statistical averaging to be reliable. In such cases, it might be possible to infer DoA information from the structure embedded in the received signals. One technique that exposes this structure is the MPM, which has been employed in FD receivers [28], [30], [32]. However, extending it to HAD receivers is fraught with difficulties, which will be addressed in Section IV below. We begin by providing a brief review of matrix pencils, the application of the MPM to FD receivers and the difficulties encountered in applying it to HAD receivers.

#### A. Review of the MPM in FD Receiver

Consider a pair of square matrices,  $(\mathbf{A}, \mathbf{B})$ , satisfying  $\mathbf{A}\mathbf{u} = \zeta\mathbf{B}\mathbf{u}$ , where the non-zero vector,  $\mathbf{u}$ , and the scalar,  $\zeta$ , are, respectively, a generalized eigenvector and a generalized eigenvalue of the pair of matrices [42], [43]. A matrix pencil

of  $(\mathbf{A}, \mathbf{B})$  is given by  $\mathbf{A} - \zeta\mathbf{B}$ . A scalar,  $\zeta$ , is a generalized eigenvalue of the pencil if and only if this value reduces the rank of the pencil. Although, originally defined for square pencils, the generalized eigenvalue problem extends to the case in which  $\mathbf{A}$  and  $\mathbf{B}$  are tall matrices [44]. Matrix pencils appear in many practical applications, including system identification [29] and DoA estimation in FD receivers [28], [30]. In these applications, the linear equations describing the system are represented by matrix pencils, with generalized eigenvalues in the form of complex exponentials representing the unknown phase parameters. To exemplify the philosophy of the MPM, we consider its application to DoA estimation in FD receivers.

To expose the pencil matrix structure embedded in the baseband signals of an FD receiver, we begin by considering a single snapshot, say the  $k$ -th one, in the noise-free case, whereupon the  $m$ -th entry of  $\mathbf{x}_k \in \mathbb{C}^M$  in (3) is given by:

$$x_k[m] = \sum_{r=1}^R s_r[k] e^{j(m-1)\mu_r}, \quad m = 1, \dots, M. \quad (11)$$

These entries are parsed into  $\xi + 1$  overlapped shifted segments of length  $M - \xi$  each, where  $\xi$  is a design parameter as discussed below [29]. Using these segments, a Hankel matrix,  $\mathbf{H}_k^{\text{FD}} \in \mathbb{C}^{(M-\xi) \times (\xi+1)}$ , is constructed as:

$$\mathbf{H}_k^{\text{FD}} = \begin{bmatrix} x_k[1] & \dots & x_k[\xi + 1] \\ \vdots & \ddots & \vdots \\ x_k[M - \xi] & \dots & x_k[M] \end{bmatrix}. \quad (12)$$

Substituting for  $\{x_k[m]\}_{m=1}^M$  from (11) in (12), it can be shown that  $\mathbf{H}_k^{\text{FD}}$  possesses a special structure, which can be used to determine the unknown DoAs. To show this, two matrices,  $\mathbf{H}_{k,1}^{\text{FD}}$  and  $\mathbf{H}_{k,2}^{\text{FD}} \in \mathbb{C}^{(M-\xi) \times \xi}$ , are obtained from each matrix  $\mathbf{H}_k^{\text{FD}}$ . In particular,  $\mathbf{H}_{k,1}^{\text{FD}}$  and  $\mathbf{H}_{k,2}^{\text{FD}}$  are obtained by deleting the last and first columns of  $\mathbf{H}_k^{\text{FD}}$ , respectively. These matrices are used to construct a matrix pencil, which will subsequently yield the unknown DoAs. Now, it can be readily verified that  $\mathbf{H}_{k,1}^{\text{FD}}$  can be written as:

$$\mathbf{H}_{k,1}^{\text{FD}} = \mathbf{\Pi}_1 \mathbf{\Lambda}_k \mathbf{\Pi}_2, \quad (13)$$

where  $\mathbf{\Pi}_1 \in \mathbb{C}^{(M-\xi) \times R}$ ,  $\mathbf{\Pi}_2 \in \mathbb{C}^{R \times \xi}$ , and  $\mathbf{\Lambda}_k \in \mathbb{C}^{R \times R}$  are:

$$\mathbf{\Pi}_1 = \begin{bmatrix} 1 & \dots & 1 \\ e^{j\mu_1} & \dots & e^{j\mu_R} \\ \vdots & \ddots & \vdots \\ e^{j(M-\xi-1)\mu_1} & \dots & e^{j(M-\xi-1)\mu_R} \end{bmatrix}, \quad (14)$$

$$\mathbf{\Pi}_2 = \begin{bmatrix} 1 & e^{j\mu_1} & \dots & e^{j(\xi-1)\mu_1} \\ \vdots & \vdots & \ddots & \vdots \\ 1 & e^{j\mu_R} & \dots & e^{j(\xi-1)\mu_R} \end{bmatrix}, \quad (15)$$

$$\mathbf{\Lambda}_k = \text{diag}(s_1[k], \dots, s_R[k]). \quad (16)$$

It is noteworthy that expression in (13) resembles a singular value decomposition (SVD) of  $\mathbf{H}_{k,1}^{\text{FD}}$ . However,  $\mathbf{\Pi}_1$  and  $\mathbf{\Pi}_2$  have a Vandermonde, rather than a unitary structure, and  $\mathbf{\Lambda}_k$  has complex, rather than positive real diagonal entries. Similar to  $\mathbf{H}_{k,1}^{\text{FD}}$ , the matrix  $\mathbf{H}_{k,2}^{\text{FD}}$  can be expressed as:

$$\mathbf{H}_{k,2}^{\text{FD}} = \mathbf{\Pi}_1 \mathbf{\Lambda}_k \mathbf{\Pi}_0 \mathbf{\Pi}_2, \quad (17)$$

where

$$\mathbf{\Pi}_0 = \text{diag}(e^{j\mu_1}, \dots, e^{j\mu_R}). \quad (18)$$

This matrix accounts for the deleted columns from  $\mathbf{H}_{k,1}^{\text{FD}}$  and  $\mathbf{H}_{k,2}^{\text{FD}}$ , and will enable the DoAs,  $\{\mu_r\}_{r=1}^R$ , to be expressed as the generalized eigenvalues of the matrix pencil constructed from these matrices. In particular, using (13) and (17), the matrix pencil  $\mathbf{H}_{k,2}^{\text{FD}} - \zeta\mathbf{H}_{k,1}^{\text{FD}}$  can be written as:

$$\mathbf{H}_{k,2}^{\text{FD}} - \zeta\mathbf{H}_{k,1}^{\text{FD}} = \mathbf{\Pi}_1 \mathbf{\Lambda}_k (\mathbf{\Pi}_0 - \zeta\mathbf{I}_R) \mathbf{\Pi}_2. \quad (19)$$

For distinct DoAs, and  $\xi \in [R, M - R]$  [31], the rank of the Vandermonde matrices,  $\mathbf{\Pi}_1$  and  $\mathbf{\Pi}_2$ , and the rank of  $\mathbf{\Lambda}_k$  is  $R$ . Hence,  $\text{rank}(\mathbf{H}_{k,2}^{\text{FD}} - \zeta\mathbf{H}_{k,1}^{\text{FD}}) = R$ , unless  $\zeta = e^{j\mu_r}$ , for some  $r \in \{1, \dots, R\}$ . In that case, the rank of the matrix pencil will be reduced by one,  $\text{rank}(\mathbf{H}_{k,2}^{\text{FD}} - \zeta\mathbf{H}_{k,1}^{\text{FD}}) = R - 1$ . Using this observation, it can be readily seen that the diagonal elements of  $\mathbf{\Pi}_0$  are the generalized eigenvalues of the matrix pair  $(\mathbf{H}_{k,2}^{\text{FD}}, \mathbf{H}_{k,1}^{\text{FD}})$ , which are the eigenvalues of

$$(\mathbf{H}_{k,1}^{\text{FD}})^\dagger \mathbf{H}_{k,2}^{\text{FD}} = \left( (\mathbf{H}_{k,1}^{\text{FD}})^H \mathbf{H}_{k,1}^{\text{FD}} \right)^{-1} (\mathbf{H}_{k,1}^{\text{FD}})^H \mathbf{H}_{k,2}^{\text{FD}}. \quad (20)$$

Using this notation, the  $r$ -th eigenvalue of  $(\mathbf{H}_{k,1}^{\text{FD}})^\dagger \mathbf{H}_{k,2}^{\text{FD}}$  is given by  $[\mathbf{\Pi}_0]_{r,r}$ , which, using (1b), yields that:

$$\hat{\theta}_r = \arcsin\left(\frac{\lambda \Im\{\log[\mathbf{\Pi}_0]_{r,r}\}}{2\pi\Delta}\right). \quad (21)$$

The aforementioned discussion shows that, in the absence of noise, MPM enables the DoAs of multiple sources to be extracted from a single snapshot, i.e.,  $K = 1$ . Next, we discuss using MPM for DoA estimation in the presence of noise.

*Using MPM in the Presence of Noise:* In the absence of noise, the rank of  $\mathbf{H}_k^{\text{FD}}$  is  $R$ . However, in the presence of independent noise components, its rank becomes  $\min(\xi + 1, M - \xi)$ , where  $\xi \in [R, M - R]$ . (Choosing  $\xi \in [\frac{M}{3}, \frac{M}{2}]$  has been recommended in [31] to minimize noise variance.) To reduce the effect of noise, the SVD of  $\mathbf{H}_k^{\text{FD}}$  can be used to discard the components associated with the noise subspace [28]–[30]. In particular,  $\mathbf{H}_k^{\text{FD}}$  can be decomposed as  $\mathbf{U}\mathbf{\Sigma}\mathbf{V}^H$ , where  $\mathbf{U}$  and  $\mathbf{V}$  are unitary matrices, and  $\mathbf{\Sigma}$  is a diagonal matrix of singular values. The left and right singular vectors in  $\mathbf{U}$  and  $\mathbf{V}$ , corresponding to the  $R$  dominant singular values, in  $\mathbf{\Sigma}$ , are retained and the remaining singular vectors and the corresponding singular values are discarded [29]. These matrices are denoted by  $\hat{\mathbf{U}}$ ,  $\hat{\mathbf{V}}$  and  $\hat{\mathbf{\Sigma}}$ . Using these matrices,  $\hat{\mathbf{H}}_k^{\text{FD}}$  is obtained as  $\hat{\mathbf{U}}\hat{\mathbf{\Sigma}}\hat{\mathbf{V}}^H$ , from which the DoAs can be estimated using the approach in Section III-A. We now consider using MPM for DoA estimation in HAD receivers.

## B. Applying the MPM in HAD Receivers

To expose the pencil structure of the baseband signals of the HAD receiver, we consider the analog combiner output signal  $\mathbf{Q}_n$  in (8). The  $k$ -th column of  $\mathbf{Q}_n$  corresponds to the  $k$ -th snapshot of the  $n$ -th segment and is given by:

$$\mathbf{q}_k = \sum_{r=1}^R \mathbf{W}_{A,n}^H \mathbf{a}_r s_r[k] + \mathbf{W}_{A,n}^H \mathbf{z}[k]. \quad (22)$$

The  $\ell$ -th entry of the vector  $\mathbf{q}_k$ ,  $q_k[\ell]$ , is given by:

$$q_k[\ell] = \sum_{r=1}^R \mathbf{w}_{A,\ell}^H \mathbf{a}_r s_r[k] + \mathbf{w}_{A,\ell}^H \mathbf{z}[k], \quad (23)$$

where  $\mathbf{w}_{A,\ell}$  is the  $\ell$ -th column of  $\mathbf{W}_{A,n}$  either FC-HAD or PC-HAD. The  $m$ -th entry of  $\mathbf{w}_{A,\ell}$  is given by  $e^{j(m-1)\phi_\ell}$ ,  $\ell, m = 1, \dots, M_{\text{RF}}$  and  $\phi_\ell$  denotes the phase shift of the analog phase shifters in the  $\ell$ -th subarray. Using this notation, we have:

$$\begin{aligned} q_k[\ell] &= \sum_{r=1}^R \sum_{m=1}^{M_{\text{RF}}} s_r[k] e^{j(\mu_r(m-1) + \psi_{r,\ell})} e^{-j\phi_\ell(m-1)} + \mathbf{w}_{A,\ell}^H \mathbf{z}[k] \\ &= \alpha \sum_{r=1}^R s_r[k] g(\mu_r - \phi_\ell) e^{j\psi_{r,\ell}} + \mathbf{w}_{A,\ell}^H \mathbf{z}[k], \ell = 1, \dots, L, \quad (24) \end{aligned}$$

where

$$g(\mu - \phi_\ell) = \frac{\sin\left(\frac{M_{\text{RF}}}{2}(\mu - \phi_\ell)\right)}{\sin\left(\frac{1}{2}(\mu - \phi_\ell)\right)} e^{j\left(\frac{(M_{\text{RF}}-1)(\mu - \phi_\ell)}{2}\right)}, \quad (25)$$

where  $\mu_r = \mu(\theta_r)$ , cf. (1b). For PC-HAD, the scalar  $\alpha = 1$  and the phase  $\psi_{r,\ell} = (\ell-1)\mu_r M_{\text{RF}}$ , whereas for FC-HAD, the scalar  $\alpha = \frac{1}{\sqrt{L}}$  due to power splitting, and the phase  $\psi_{r,\ell} = 0$ .

We now elaborate on the difficulties encountered when applying MPM for DoA estimation in HAD receivers. Towards that end, one would be tempted to follow a path analogous to that used for FD receivers. To show that HAD receivers are not amenable to this path, we note that, in FD receivers, the DoA-bearing signals  $\{x_k[m]\}_{m=1}^M$  in (11) are directly available for baseband processing. In contrast, in HAD receivers, only the signals  $\{q_k[\ell]\}_{\ell=1}^L$  in (24), the output of the analog combiner, are accessible for baseband processing. Comparing the structure of  $x_k[m]$  with that of  $q_k[\ell]$ , we observe that, whereas the baseband signals,  $\{s_r\}_{r=1}^R$ , and the DoAs embedded in the phases  $\{\mu_r\}_{r=1}^R$  of the  $R$  sources are directly available in  $\{x_k[m]\}_{m=1}^M$ , these signals and phases are not directly recoverable from the signals  $\{q_k[\ell]\}_{\ell=1}^L$ . To see that, we note that, in  $q_k[\ell]$ , the baseband signals,  $\{s_r\}_{r=1}^R$ , are scaled by  $\alpha|g(\mu_r - \phi_\ell)|$  and the phases  $\{\mu_r\}_{r=1}^R$  are shifted by the phase shifts,  $\{\phi_\ell\}_{\ell=1}^L$ , of the analog combiner. As such, following the path used to apply the MPM to FD receivers in their HAD counterparts would require constructing a Hankel matrix with  $q_k[\ell]$  signals in (24) analogous to the FD one in (12). This matrix must be amenable to a decomposition analogous to the one in (12) and the unknown phases  $\{\mu_r\}_{r=1}^R$  must be amenable to be isolated in a diagonal matrix analogous to  $\mathbf{\Pi}_0$  in (18). Unfortunately, when the phase shifts of the analog combiner are not identical, the Hankel matrix constructed from the  $\{q_k[\ell]\}_{\ell=1}^L$  signals cannot be decomposed in a manner analogous to the ones in (13) and (17). In particular, the signal on which MPM is applied depends not only on the unknown phases  $\{\mu_r\}_{r=1}^R$  but also on the phases  $\{\phi_\ell\}_{\ell=1}^L$ . These phases disrupt the matrix structure, rendering the construction of a pencil akin to the one used in FD receivers infeasible. Hence, using matrix pencils to extract the unknown DoAs in HAD receivers requires fundamentally different approaches.

In addition to the difficulties of applying MPM to HAD receivers, the HAD structure suffers from another limitation [36], which follows from processing the received signals

by the  $M \times L$  analog combiner matrix  $\mathbf{W}_{A,n}$ , cf. (8). Since in these receivers  $L < M$ , it can be seen that the  $\mathbf{W}_{A,n}$  projects the received signal vector on a particular subspace spanned by the column vectors of  $\mathbf{W}_{A,n}$ . Thus, an analog combiner defines spatial sectors for which the DoAs can be estimated. Outside these sectors, the received signal would be heavily attenuated or even nullified. To address these challenges, we next propose two approaches centered around the MPM.

#### IV. PROPOSED MPM-BASED APPROACHES FOR DOA ESTIMATION IN HAD RECEIVERS

In this section, we develop two MPM-based approaches for DoA estimation in HAD receivers. These approaches will result in Hankel matrices that can be used to extract the DoAs using the MPM. These approaches will also eliminate the potential of heavy attenuation which the received signals may be subjected to, otherwise. We begin by considering the noiseless case with a single snapshot and then extend these approaches to multiple snapshots in the presence of noise.

##### A. Full Coverage and Periodicity-Based MPM (PMPM)

The first proposed approach addresses the attenuation incurred by the analog combiner by cycling over an exhaustive set of analog combiners that collectively span the entire space. This approach then uses the periodic, potentially unknown, deterministic components, such as training pilots or preamble segments of the received signal frames, typically used in communication protocols [41]. We will show that access to such signals can be used to combine and disentangle the signals at the outputs of the analog combiners. Hence, HAD receivers, either FC or PC, can feature behavior that resembles that of FD receivers, and DoA can be estimated using the MPM. We begin with a scheme to ensure full spatial coverage.

1) *A Set of Exhaustive Analog Combiners*: In HAD receivers, the analog combiner represents a spatial sector within which the DoAs can be estimated. Received signals with DoAs outside this sector will be attenuated, or even nullified. To avoid this limitation, we follow the scheme advocated in [36]. In this scheme, an exhaustive set of analog combiners is used to collectively span the entire space. It was argued in [36] that, in order to span a subspace with the largest possible dimension, the matrix  $\mathbf{W}_A$  must be full column rank, i.e.,  $L$ . Towards that end, we construct the analog combiners of FC-HAD receivers from distinct columns of the DFT matrix, and we construct those of PC-HAD receivers using a single column of the DFT matrix for each of those combiners. This construction of PC-HAD analog combiners contrasts that proposed in [36], wherein the diagonal blocks are constructed from distinct, rather than identical, columns of the DFT matrix. Using identical columns of the DFT matrix in the PC-HAD analog combiners will enable using the MPM to extract the DoAs embedded in the received signals, cf. Sections IV-A2–IV-B below. To elaborate, we consider the  $M_{\text{RF}}$ -point DFT matrix which is denoted by  $\mathbf{V}_{M_{\text{RF}}} = [\mathbf{v}_1, \dots, \mathbf{v}_{M_{\text{RF}}}]$ , where the  $m$ -th entry of  $\mathbf{v}_\ell$  is given by  $e^{j(m-1)\phi_\ell}$ ,  $\phi_\ell = \frac{2\pi(\ell-1)}{M_{\text{RF}}}$ ,  $\ell, m = 1, \dots, M_{\text{RF}}$ . Using  $\mathbf{V}_{M_{\text{RF}}}$  to construct the HAD analog combiners ensures not only that all non-zero entries are unit

modulus, but also that analog combiners are full column rank, which will facilitate subsequent mathematical manipulation.

For FC-HAD,  $M_{\text{RF}} = M$ . In this case, an exhaustive set of analog combiners,  $\{\mathbf{W}_{\text{AFC},n}\}_{n=1}^N$ ,  $N = \frac{M}{L}$ , can be constructed by choosing each  $\mathbf{W}_{\text{AFC},n}$  to contain  $L$  distinct columns of the  $M_{\text{RF}}$ -point DFT matrix, for  $n \in \{1, \dots, N\}$ , i.e.,

$$\mathbf{W}_{\text{AFC},n} = \frac{1}{\sqrt{L}} [\mathbf{v}_{(n-1)L+1} \ \cdots \ \mathbf{v}_{nL}]. \quad (26)$$

The matrix  $\mathbf{W}_{\text{AFC},n}$  processes the  $n$ -th segment containing  $K$  snapshots, assuming that the total number of snapshots is  $NK$ . The set of phases used by  $\mathbf{W}_{\text{AFC},n}$ , is  $\mathcal{V}_n = \left\{ \frac{2\pi(n-1)L}{M_{\text{RF}}}, \dots, \frac{2\pi(nL-1)}{M_{\text{RF}}} \right\}$  for  $n \in \{1, \dots, \frac{N}{2}\}$  and  $\mathcal{V}_n = \left\{ \frac{2\pi(n-1)L}{M_{\text{RF}}} - 2\pi, \dots, \frac{2\pi(nL-1)}{M_{\text{RF}}} - 2\pi \right\}$  for  $n \in \{\frac{N}{2}+1, \dots, N\}$ . This set of analog combiners spans the entire space.

For PC-HAD,  $M_{\text{RF}} = \frac{M}{L}$  and the analog combiners possess a block diagonal structure. Hence, in this case, it suffices for an exhaustive set of analog combiners,  $\{\mathbf{W}_{\text{APC},n}\}_{n=1}^N$ ,  $N = \frac{M}{L}$ , to be such that each of the matrices in the set is constructed from a single column of the DFT matrix. In other words,  $\mathbf{W}_{\text{APC},n}$  takes the form in (10), but with  $\mathbf{w}_{\text{APC},\ell} = \mathbf{v}_n$ , for  $n, \ell \in \{1, \dots, M_{\text{RF}}\}$ , i.e.,

$$\mathbf{W}_{\text{APC},n} = \bigoplus_{\ell=1}^L \mathbf{v}_n. \quad (27)$$

The  $m$ -th entry of  $\mathbf{v}_n$  is  $e^{j(m-1)\phi_n}$ , and

$$\phi_n = \begin{cases} \frac{2\pi(n-1)}{M_{\text{RF}}}, & n \in \{1, \dots, \frac{M_{\text{RF}}}{2}\}, \\ \frac{2\pi(n-1)}{M_{\text{RF}}} - 2\pi, & n \in \{\frac{M_{\text{RF}}}{2} + 1, \dots, M_{\text{RF}}\}. \end{cases} \quad (28)$$

As in the case of FC-HAD, in PC-HAD, the matrix  $\mathbf{W}_{\text{APC},n}$  processes the  $n$ -th segment containing  $K$  snapshots, and the set  $\{\mathbf{W}_{\text{APC},n}\}_{n=1}^N$  spans the entire  $M_{\text{RF}}$ -dimensional space.

Figures 2a and 2b illustrate  $\frac{|g(\mu_r - \phi_\ell)|}{\sqrt{L}}$ , defined in (25), for FC-HAD with  $M_{\text{RF}} = 8$  and  $L = 2$ . The scaling  $\frac{1}{\sqrt{L}}$  arises from power splitting. In particular, Figure 2a corresponds to  $\mathbf{W}_{\text{AFC},n}$  constructed using the first two columns of  $\mathbf{V}_8$ , whereas Figure 2b corresponds to  $\{\mathbf{W}_{\text{AFC},n}\}_{n=1}^N$  constructed using all columns of  $\mathbf{V}_8$ . Similarly, Figures 2c and 2d illustrate  $|g(\mu - \phi_n)|$  for PC-HAD, with  $M_{\text{RF}} = 4$  and  $L = 2$ . Figure 2c shows  $|g(\mu - \phi_n)|$  corresponding to  $\mathbf{W}_{\text{APC},n}$  constructed using the first column of  $\mathbf{V}_4$ , whereas Figure 2d corresponds to  $\{\mathbf{W}_{\text{APC},n}\}_{n=1}^N$  constructed using all columns of  $\mathbf{V}_4$ .

The fact that both  $\{\mathbf{W}_{\text{AFC},n}\}_{n=1}^N$  and  $\{\mathbf{W}_{\text{APC},n}\}_{n=1}^N$  span the entire space ensures that signals arriving from all DoAs in  $[-\frac{\pi}{2}, \frac{\pi}{2}]$  are not heavily attenuated or nullified by either the FC-HAD or the PC-HAD analog combiner.

Having described the set of  $N$  orthogonal analog combiners, we next introduce our first approach to address the difficulties in applying the MPM in HAD receivers.

2) *PMPM Approach*: In Section III-B, we showed that applying the MPM in HAD receivers entangles the output signals, rendering MPM invocation unwieldy. One approach to remedy this difficulty is presented in the following theorem.

*Theorem 1*: Let  $\{\mathbf{W}_{\text{A},n}\}_{n=1}^N$  be a set of analog combiners, each satisfying  $\mathbf{W}_{\text{A},n}^H \mathbf{W}_{\text{A},n} = \alpha^2 M_{\text{RF}} \mathbf{I}_L$ . Let the number of snapshots processed by  $\mathbf{W}_{\text{A},n}$  be  $K$  and let the signal

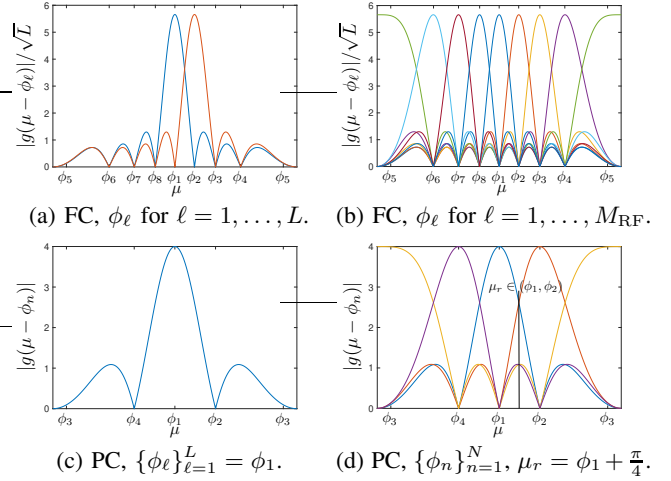


Figure 2: Illustration of (25) with  $M = 8$ ,  $L = 2$ ,  $N = 4$  and  $M_{\text{RF}} = 8$  in FC-HAD and  $M_{\text{RF}} = 4$  in PC-HAD.

$\mathbf{S}_n$  in (8) be periodic, i.e.,  $\mathbf{S}_n = \mathbf{S}$ . Let  $\{\mathbf{W}_{\text{D},n}\}_{n=1}^N$  be a set of  $N$  baseband digital combiners, each processes the output of the  $n$ -th analog combiner,  $\mathbf{Q}_n$  in (8). Setting  $\mathbf{W}_{\text{D},n} = \frac{1}{\alpha^2 M_{\text{RF}}} \mathbf{W}_{\text{A},n}^H \in \mathbb{C}^{L \times M}$  yields an aggregate output of the  $N$  combiners,  $\mathbf{Y}_{\text{PMPM}} \in \mathbb{C}^{M \times K}$ , which is given by:

$$\mathbf{Y}_{\text{PMPM}} = \mathbf{A}\mathbf{S} + \sum_{n=1}^N \mathbf{P}_{\mathbf{W}_{\text{A},n}} \mathbf{Z}_n, \quad (29)$$

where  $\mathbf{P}_{\mathbf{W}_{\text{A},n}} = \frac{1}{\alpha^2 M_{\text{RF}}} \mathbf{W}_{\text{A},n} \mathbf{W}_{\text{A},n}^H$ . The signal  $\mathbf{Y}_{\text{PMPM}}$  is equivalent to the  $K$ -snapshot input signal,  $\mathbf{X}$ , of the FD receiver in (4). The SNR of both  $\mathbf{Y}_{\text{PMPM}}$  and  $\mathbf{X}$  is  $\frac{1}{M} \text{Tr}(\mathbf{A}\Phi\mathbf{A}^H)$ . In particular,

$$\mathbf{Y}_{\text{PMPM}} \Big|_{\bar{K}=NK} = \mathbf{X} \Big|_{\bar{K}=K}. \quad (30)$$

*Proof*: See Appendix A. ■

From this theorem, it can be seen that DoAs that are recoverable by the FD receiver, are also recoverable by the HAD receiver using the PMPM approach, at the same the signal power but with  $N$ -fold the number of snapshots. In particular, PMPM ensures that no signal is nullified by projection, irrespective of its DoA. This is achieved in PMPM by using  $N$ , rather than one snapshot as in the FD case.

We note that the periodicity requirement in Theorem 1 can be satisfied in commonly deployed communication systems, e.g., 5G+, in which the frame contains repeated preamble segments or training pilots. It is also worth noting that the periodic snapshots may not be contiguous for the PMPM approach to apply. For instance, the periodic preamble segments may be separated by non-periodic payloads. Furthermore, these periodic signals do not need to be known *a priori*, nor do they need to be detected for the PMPM approach to be applied. However, exploiting signal periodicity requires the HAD receiver to be synchronized.

Having developed a technique for making the output of the digital combiners of the HAD receiver equivalent to that of its FD counterpart, we are now in a position to apply the MPM to estimate the DoAs in a manner analogous to FD receivers.

To apply the MPM in HAD receivers, we begin by considering the  $k$ -th column of  $\mathbf{Y}_{\text{PMPM}}$ ,  $\mathbf{y}_k \in \mathbb{C}^M$ .<sup>2</sup> We construct the Hankel matrix  $\mathbf{H}_k^{\text{PMPM}} \in \mathbb{C}^{(M-\xi) \times (\xi+1)}$ ,

$$\mathbf{H}_k^{\text{PMPM}} = \begin{bmatrix} y_k[1] & \cdots & y_k[\xi+1] \\ \vdots & \ddots & \vdots \\ y_k[M-\xi] & \cdots & y_k[M] \end{bmatrix}. \quad (31)$$

Analogous to the FD case, a matrix pencil in the proposed PMPM approach can be synthesized from the two matrices,  $\mathbf{H}_{k,1}^{\text{PMPM}}$  and  $\mathbf{H}_{k,2}^{\text{PMPM}}$ , which are obtained by deleting the last and first columns of  $\mathbf{H}_k^{\text{PMPM}}$ , respectively. As in the FD case, we write  $\mathbf{H}_{k,1}^{\text{PMPM}} = \mathbf{\Pi}_1 \mathbf{\Lambda}_k \mathbf{\Pi}_2$  and  $\mathbf{H}_{k,2}^{\text{PMPM}} = \mathbf{\Pi}_1 \mathbf{\Lambda}_k \mathbf{\Pi}_0 \mathbf{\Pi}_2$ , where  $\mathbf{\Pi}_1 \in \mathbb{C}^{(M-\xi) \times R}$ ,  $\mathbf{\Pi}_2 \in \mathbb{C}^{R \times \xi}$ ,  $\mathbf{\Lambda}_k$ , and  $\mathbf{\Pi}_0 \in \mathbb{C}^{R \times R}$  are given in (14), (15), (16), and (18), respectively. Analogous to FD, the diagonal elements of  $\mathbf{\Pi}_0$  are the generalized eigenvalues of the matrix pair  $(\mathbf{H}_{k,2}^{\text{PMPM}}, \mathbf{H}_{k,1}^{\text{PMPM}})$ , which are the eigenvalues of  $(\mathbf{H}_{k,1}^{\text{PMPM}})^\dagger \mathbf{H}_{k,2}^{\text{PMPM}}$ . In particular, the  $r$ -th diagonal entry of  $\mathbf{\Pi}_0$ ,  $[\mathbf{\Pi}_0]_{r,r}$ , is equal to the  $r$ -th eigenvalue of  $(\mathbf{H}_{k,1}^{\text{PMPM}})^\dagger \mathbf{H}_{k,2}^{\text{PMPM}}$ . Substituting this eigenvalue in (21) yields the  $r$ -th DoA,  $r = 1, \dots, R$ .

Having considered one column of  $\mathbf{Y}_{\text{PMPM}}$  in the noise-free case, we now consider applying the PMPM to multiple columns of  $\mathbf{Y}_{\text{PMPM}}$  in the presence of noise.

3) *Multiple Snapshots in the Presence of Noise:* In this section, we apply the MPM when multiple (actual, as in FD, or virtual as in HAD) snapshots are considered simultaneously.

a) *Noiseless Case:* The MPM hinges on the decompositions in (13) and (17). Hence, to apply it when multiple snapshots are available to the receiver, a Hankel-based construction is needed to enable a matrix pencil with generalized eigenvalues corresponding to the desired DoAs. One approach to do so was alluded to in [32]. In particular, each actual or virtual snapshot is used to construct a Hankel matrix and a collection of such matrices is concatenated in one augmented matrix, which we denote by  $\mathbf{H}_A \in \mathbb{C}^{(M-\xi) \times K_A(\xi+1)}$ . This collection contains  $K_A$  matrices, where  $K_A = \tilde{K}$  for FD and  $K_A = \frac{\tilde{K}}{N}$  for HAD using PMPM. The augmented matrix is:

$$\mathbf{H}_A = [\mathbf{H}_1 \quad \cdots \quad \mathbf{H}_{K_A}]. \quad (32)$$

Towards using  $\mathbf{H}_A$  to extract the DoAs, we introduce the notation  $\mathbf{H}_{A,-\ell}$  to represent a matrix identical to  $\mathbf{H}_A$  but with the  $\ell$ -th column removed. In particular, to construct a matrix pencil, two Hankel-based matrices  $\mathbf{H}_{A,-\mathcal{I}}$  and  $\mathbf{H}_{A,-\mathcal{J}} \in \mathbb{C}^{(M-\xi) \times K_A \xi}$  are obtained from  $\mathbf{H}_A$  as follows:

$$\mathbf{H}_{A,-\mathcal{I}} = [\mathbf{H}_{1,-(\zeta+1)} \quad \cdots \quad \mathbf{H}_{K_A,-(\zeta+1)}], \quad (33)$$

$$\mathbf{H}_{A,-\mathcal{J}} = [\mathbf{H}_{1,-1} \quad \cdots \quad \mathbf{H}_{K_A,-1}], \quad (34)$$

where the sets  $\mathcal{I} = \{i(\xi+1)\}_{i=1}^{K_A}$  and  $\mathcal{J} = \{(j-1)(\xi+1)+1\}_{j=1}^{K_A}$  identify the column indices to be removed from  $\mathbf{H}_A$  to construct  $\mathbf{H}_{A,-\mathcal{I}}$  and  $\mathbf{H}_{A,-\mathcal{J}}$ , respectively. Using the embedded Hankel structure, we can write:

$$\mathbf{H}_{A,-\mathcal{I}} = \mathbf{\Pi}_{A,1} \mathbf{\Lambda}_A \mathbf{\Pi}_{A,2}, \quad (35)$$

$$\mathbf{H}_{A,-\mathcal{J}} = \mathbf{\Pi}_{A,1} \mathbf{\Lambda}_A (\mathbf{I}_{K_A} \otimes \mathbf{\Pi}_0) \mathbf{\Pi}_{A,2}, \quad (36)$$

<sup>2</sup>The  $k$ -th column of  $\mathbf{Y}_{\text{PMPM}}$ ,  $\mathbf{y}_k$ , represents a virtual snapshot for HAD receivers using PMPM and an actual snapshot,  $\mathbf{x}_k$ , in the FD receiver, cf. (3).

where  $\mathbf{\Pi}_{A,1} = \mathbf{1}_{K_A}^T \otimes \mathbf{\Pi}_1 \in \mathbb{C}^{(M-\xi) \times (K_A \times R)}$ ,  $\mathbf{\Pi}_{A,2} = \mathbf{I}_{K_A} \otimes \mathbf{\Pi}_2 \in \mathbb{C}^{(K_A \times R) \times (K_A \times \xi)}$ , and  $\mathbf{\Lambda}_A = \bigoplus_{k=1}^{K_A} \mathbf{\Lambda}_k \in \mathbb{C}^{(K_A \times R) \times (K_A \times R)}$ . Similar to FD, the matrix  $\mathbf{\Pi}_0$  accounts for the deleted columns from  $\mathbf{H}_{A,-\mathcal{I}}$  and  $\mathbf{H}_{A,-\mathcal{J}}$ , and enables the DoAs,  $\{\mu_r\}_{r=1}^R$ , to be expressed as the generalized eigenvalues of the matrix pencil constructed from these matrices. In particular, using (35) and (36), the matrix pencil  $\mathbf{H}_{A,-\mathcal{J}} - \zeta \mathbf{H}_{A,-\mathcal{I}}$ , which has a rank  $R$ , can be written as:

$$\mathbf{H}_{A,-\mathcal{J}} - \zeta \mathbf{H}_{A,-\mathcal{I}} = \mathbf{\Pi}_{A,1} \mathbf{\Lambda}_A (\mathbf{I}_{K_A} \otimes (\mathbf{\Pi}_0 - \zeta \mathbf{I}_R)) \mathbf{\Pi}_{A,2}. \quad (37)$$

It can be readily seen that the diagonal elements of  $\mathbf{\Pi}_0$  are the generalized eigenvalues of the matrix pair  $(\mathbf{H}_{A,-\mathcal{J}}, \mathbf{H}_{A,-\mathcal{I}})$ , corresponding to the eigenvalues of  $(\mathbf{H}_{A,-\mathcal{I}})^\dagger \mathbf{H}_{A,-\mathcal{J}}$ , that is, the  $r$ -th eigenvalue of  $(\mathbf{H}_{A,-\mathcal{I}})^\dagger \mathbf{H}_{A,-\mathcal{J}}$  equals  $[\mathbf{\Pi}_0]_{r,r}$ . It is worth noting that MPM requires only a single snapshot to extract the DoAs. In the noiseless case, multiple snapshots provide no extra information. However, in the presence of noise, multiple snapshots can be exploited to improve estimation accuracy, as discussed next.

b) *Noisy Case:* Analogous to the FD case, the noise subspace can be discarded by invoking the SVD of  $\mathbf{H}_A$  in (32), cf. Section III-A. In particular,  $\mathbf{H}_A$  can be decomposed as  $\mathbf{U}_A \mathbf{\Sigma}_A \mathbf{V}_A^H$ , where  $\mathbf{U}_A \in \mathbb{C}^{(M-\xi) \times (M-\xi)}$  and  $\mathbf{V}_A \in \mathbb{C}^{K_A(\xi+1) \times (M-\xi)}$  are unitary matrices, and  $\mathbf{\Sigma}_A \in \mathbb{C}^{(M-\xi) \times (M-\xi)}$  is a diagonal matrix containing the singular values of  $\mathbf{H}_A$ . The left and right-singular vectors in  $\mathbf{U}_A$  and  $\mathbf{V}_A$  corresponding to the largest  $R$  singular values, in  $\mathbf{\Sigma}_A$ , are retained and the remaining singular vectors and the corresponding singular values are discarded. These matrices represent the signal components in the signal subspace after eliminating the noise subspace and are denoted by  $\hat{\mathbf{U}}_A \in \mathbb{C}^{(M-\xi) \times R}$ ,  $\hat{\mathbf{V}}_A \in \mathbb{C}^{K_A(\xi+1) \times R}$  and  $\hat{\mathbf{\Sigma}}_A \in \mathbb{C}^{R \times R}$ . Using these matrices, the matrix  $\hat{\mathbf{H}}_A$  is obtained as  $\hat{\mathbf{U}}_A \hat{\mathbf{\Sigma}}_A \hat{\mathbf{V}}_A^H$ . Using  $\hat{\mathbf{H}}_A$ , we follow the procedure outlined in the noiseless case to obtain the two matrices  $\hat{\mathbf{H}}_{A,-\mathcal{I}}$  and  $\hat{\mathbf{H}}_{A,-\mathcal{J}}$ , cf. (33) and (34). The matrices  $\hat{\mathbf{H}}_{A,-\mathcal{I}}$  and  $\hat{\mathbf{H}}_{A,-\mathcal{J}}$ , being synthesized from the singular vectors and the  $R$  largest singular values, no longer possess the Hankel structure. However, the generalized eigenvalues of the matrix pair  $(\hat{\mathbf{H}}_{A,-\mathcal{J}}, \hat{\mathbf{H}}_{A,-\mathcal{I}})$ , i.e., the eigenvalues of  $(\hat{\mathbf{H}}_{A,-\mathcal{I}})^\dagger \hat{\mathbf{H}}_{A,-\mathcal{J}}$ ,  $\{\nu_r\}_{r=1}^R$ , constitute an approximation of the diagonal elements of  $\mathbf{\Pi}_0$  [45]. Using this approximation, DoA estimates,  $\{\hat{\theta}_r\}_{r=1}^R$ , can be obtained as:

$$\hat{\theta}_r = \arcsin \left( \frac{\lambda \Im \left\{ \log(\nu_r ((\hat{\mathbf{H}}_{A,-\mathcal{I}})^\dagger \hat{\mathbf{H}}_{A,-\mathcal{J}})) \right\}}{2\pi \Delta} \right). \quad (38)$$

Increasing the number of snapshots increases the spread of the singular values corresponding to the signal subspace and those corresponding to the noise subspace. This subsequently results in enhancing the DoA estimation accuracy, as will be demonstrated numerically in Section V below.

Despite its effectiveness, the PMPM approach depends on segments of the received signal being periodic, which requires synchronization and may not be always possible. To address these limitations, a second approach that does not rely on signal periodicity is proposed next.

### B. Single-Phase PC Analog Combiners for MPM (SPC-MPM)

To eliminate the contingency on periodic signals characteristic of the approach proposed in Section IV-A, we now propose another approach that capitalizes on the block diagonal structure of the analog combiners of PC-HAD receivers. The second approach is introduced in the following theorem.

*Theorem 2:* Let  $\{\mathbf{W}_{\text{APC},n}\}_{n=1}^N$  be a set of PC-HAD analog combiners defined in (27), such that  $\mathbf{W}_{\text{APC},n}^H \mathbf{W}_{\text{APC},n} = M_{\text{RF}} \mathbf{I}_L$ ,  $n = 1, \dots, N$ , and  $\sum_{n=1}^N \frac{1}{M_{\text{RF}}} \mathbf{W}_{\text{A},n} \mathbf{W}_{\text{A},n}^H = \mathbf{I}_M$ . If the number of snapshots processed by the set of analog combiners is denoted by  $NK$ , then the output of  $\{\mathbf{W}_{\text{APC},n}\}_{n=1}^N$ ,  $\{\mathbf{Q}_n\}_{n=1}^N$  of the  $M$ -antenna PC-HAD receiver is equivalent to the input of an FD receiver that: 1) has  $L$  antennas with spacing  $\Delta_{\text{SPC}} = M_{\text{RF}}\Delta$ , 2) uses  $K$  snapshots, and 3) requires an SNR of the  $r$ -th source that is at least  $10 \log M_{\text{RF}} \sin^2\left(\frac{\pi}{2M_{\text{RF}}}\right)$  dB higher than the corresponding SNR of the PC-HAD receiver. In particular,

$$\left\{ \mathbf{Q}_n \right\}_{n=1}^N \Big|_{\tilde{K}=NK} \Big|_{\text{SNR}_{\text{SPC},r} \in \left[ \frac{P_r}{M_{\text{RF}} \sin^2(\pi/(2M_{\text{RF}}))}, M_{\text{RF}} P_r \right]} = \mathbf{X} \Big|_{\tilde{K}=K} \Big|_{\text{SNR}_{\text{FD},r}=P_r}. \quad (39)$$

*Proof:* See Appendix B.  $\blacksquare$

*Remark 1:* The lower bound of  $\text{SNR}_{\text{SPC},r}$  in (39) increases monotonically with  $M_{\text{RF}}$ . Hence, this bound asymptotically approaches  $10 \log \frac{4}{\pi^2} M_{\text{RF}} P_r$  dB as  $M_{\text{RF}} \rightarrow \infty$ .  $\square$

The equivalence of  $\mathbf{Q}_n$  and  $\mathbf{X}$  elucidated in Theorem 2 shows that setting  $\mathbf{w}_{\text{APC},\ell} = \mathbf{v}_n$  enables the MPM to extract the DoAs in the PC-HAD architecture, albeit with the snapshot penalty and SNR gain outlined in the theorem.

To apply the MPM, we assume that  $\theta_r \in \Theta_n$ , the spatial sector covered by  $\mathbf{W}_{\text{APC},n}$ . We begin by considering a single snapshot of the signal arriving from this DoA, i.e., the  $k$ -th column of  $\mathbf{Q}_n$  in (8),  $\mathbf{q}_k \in \mathbb{C}^{L \times 1}$ , in the noise-free case. The Hankel matrix,  $\mathbf{H}_k^{\text{SPC}} \in \mathbb{C}^{(L-\xi) \times (\xi+1)}$ , is constructed as:

$$\mathbf{H}_k^{\text{SPC}} = \sum_{r=1}^R \begin{bmatrix} s_r[k]g(\mu_r - \phi_n)e^{j\psi_{r,1}} & \cdots & s_r[k]g(\mu_r - \phi_n)e^{j\psi_{r,(\xi+1)}} \\ \vdots & \ddots & \vdots \\ s_r[k]g(\mu_r - \phi_n)e^{j\psi_{r,L-\xi}} & \cdots & s_r[k]g(\mu_r - \phi_n)e^{j\psi_{r,L}} \end{bmatrix}. \quad (40)$$

Analogous to FD and PMPM, a matrix pencil in the SPC-MPM approach can be synthesized from the two matrices,  $\mathbf{H}_{k,1}^{\text{SPC}}$  and  $\mathbf{H}_{k,2}^{\text{SPC}} \in \mathbb{C}^{(L-\xi) \times \xi}$ , which are obtained by deleting the last and first columns of  $\mathbf{H}_k^{\text{SPC}}$ , respectively. Hence,  $\mathbf{H}_{k,1}^{\text{SPC}}$  and  $\mathbf{H}_{k,2}^{\text{SPC}}$  can be expressed as:

$$\mathbf{H}_{k,1}^{\text{SPC}} = \mathbf{\Pi}_1^{\text{SPC}} \mathbf{\Lambda}_k^{\text{SPC}} \mathbf{\Pi}_2^{\text{SPC}}, \quad (41)$$

$$\mathbf{H}_{k,2}^{\text{SPC}} = \mathbf{\Pi}_1^{\text{SPC}} \mathbf{\Lambda}_k^{\text{SPC}} \mathbf{\Pi}_0^{\text{SPC}} \mathbf{\Pi}_2^{\text{SPC}}, \quad (42)$$

where  $\mathbf{\Pi}_1^{\text{SPC}} \in \mathbb{C}^{(L-\xi) \times R}$ ,  $\mathbf{\Pi}_2^{\text{SPC}} \in \mathbb{C}^{R \times \xi}$ ,  $\mathbf{\Pi}_0^{\text{SPC}}$  and  $\mathbf{\Lambda}_k^{\text{SPC}} \in \mathbb{C}^{R \times R}$  are given by:

$$\mathbf{\Pi}_1^{\text{SPC}} = \begin{bmatrix} 1 & \cdots & 1 \\ e^{jM_{\text{RF}}\mu_1} & \cdots & e^{jM_{\text{RF}}\mu_R} \\ \vdots & \ddots & \vdots \\ e^{j(L-\xi-1)M_{\text{RF}}\mu_1} & \cdots & e^{j(L-\xi-1)M_{\text{RF}}\mu_R} \end{bmatrix}, \quad (43)$$

$$\mathbf{\Pi}_2^{\text{SPC}} = \begin{bmatrix} 1 & e^{jM_{\text{RF}}\mu_1} & \cdots & e^{j(\xi-1)M_{\text{RF}}\mu_1} \\ \vdots & \vdots & \ddots & \vdots \\ 1 & e^{jM_{\text{RF}}\mu_R} & \cdots & e^{j(\xi-1)M_{\text{RF}}\mu_R} \end{bmatrix}, \quad (44)$$

$$\mathbf{\Pi}_0^{\text{SPC}} = \text{diag}(e^{jM_{\text{RF}}\mu_1}, \dots, e^{jM_{\text{RF}}\mu_R}), \quad (45)$$

$$\mathbf{\Lambda}_k^{\text{SPC}} = \text{diag}(s_1[k]g(\mu_1 - \phi_n), \dots, s_R[k]g(\mu_R - \phi_n)). \quad (46)$$

The diagonal elements of  $\mathbf{\Pi}_0^{\text{SPC}}$  are the generalized eigenvalues of the matrix pair  $(\mathbf{H}_{k,2}^{\text{SPC}}, \mathbf{H}_{k,1}^{\text{SPC}})$ , i.e., the eigenvalues of  $(\mathbf{H}_{k,1}^{\text{SPC}})^\dagger \mathbf{H}_{k,2}^{\text{SPC}}$ . Hence, using (1b) yields the following estimate of the  $r$ -th DoA:

$$\hat{\theta}_r = \arcsin\left(\frac{\lambda \Im\{\log[\mathbf{\Pi}_0^{\text{SPC}}]_{r,r}\}}{2\pi M_{\text{RF}}\Delta}\right). \quad (47)$$

Since the spatial sector in which  $\theta_r$  lies is not known *a priori*,  $r = 1, \dots, R$ , the entire space must be covered by an exhaustive set of analog combiners. One such set is defined in (27). Now, for  $K$  snapshots to be received from each DoA, the total number of snapshots must be  $\tilde{K} = NK$ ;  $\tilde{K}$  should be, at least, equal to  $N$ . To use  $K$  snapshots per analog combiner to extract the DoAs, a technique analogous to the one outlined in Section IV-A3a can be used with the SPC-MPM approach. In particular, a Hankel matrix, i.e.,  $\mathbf{H}_k^{\text{SPC}}$  in (40), is constructed for each snapshot. The collection of  $K_A = \tilde{K}$  matrices corresponding to  $\tilde{K}$  snapshots are concatenated into the augmented matrix  $\mathbf{H}_A$  in (32). The Hankel matrices constructed from the  $K$  snapshots of the  $n$ -th analog combiner, i.e.,  $\mathbf{H}_A \in \mathbb{C}^{(L-\xi) \times K_A(\xi+1)}$  can be rewritten as:

$$\mathbf{H}_A = \left[ \underbrace{\mathbf{H}_1 \cdots \mathbf{H}_K}_{\text{correspond to } \mathbf{W}_{\text{APC},1}} \cdots \underbrace{\mathbf{H}_{K_A-K+1} \cdots \mathbf{H}_{K_A}}_{\text{correspond to } \mathbf{W}_{\text{APC},N}} \right]. \quad (48)$$

A matrix pencil is constructed using two Hankel-based matrices  $\mathbf{H}_{A,-\mathcal{I}}$  and  $\mathbf{H}_{A,-\mathcal{J}} \in \mathbb{C}^{(L-\xi) \times K_A \xi}$ , which are obtained from  $\mathbf{H}_A$  in (48) as in (33) and (34). Expressing these matrices in the forms of (35) and (36) enables extracting the DoAs using the MPM outlined in Section IV-A3a with  $\mathbf{\Pi}_1^{\text{SPC}}$ ,  $\mathbf{\Pi}_2^{\text{SPC}}$ ,  $\mathbf{\Pi}_0^{\text{SPC}}$  and  $\mathbf{\Lambda}_k^{\text{SPC}}$  defined in (43), (44), (45) and (46), respectively. Note that, unlike FD and the PMPM approach in HAD receivers, the number of antennas is virtually equal to  $L$  rather than  $M$ . Finally, in the presence of noise, the technique in Section IV-A3b can be used to estimate the DoAs using (38) but with  $\Delta \leftarrow M_{\text{RF}}\Delta$ .

*Remark 2:* A limitation of the SPC-MPM DoA estimation approach is that it relies only on the phase information,  $\psi_{r,\ell} = (\ell - 1)\mu_r M_{\text{RF}}$ , embedded in  $\mathbf{Q}_n$ , but does not exploit the amplitude and phase information embedded in  $g(\mu_r - \phi_n)$ . Although exploiting this information could potentially improve the estimation accuracy, such improvement is likely marginal because the gap between the variance of the estimates generated by the SPC-MPM approach and the corresponding CRLB is typically small, as demonstrated in Section V below.  $\square$

*Remark 3:* The lower bound on  $\text{SNR}_{\text{SPC},r}$  in Theorem 2 is derived when the output of only one analog combiner is used for DoA estimation. Since the output of all analog combiners,  $\{\mathbf{W}_{\text{APC},n}\}_{n=1}^N$ , contain DoA information, a strictly higher SNR can be achieved by concatenating the corresponding Hankel matrices as in (48).  $\square$

*Corollary 1:* If the spacing between the antennas of the original array is  $\Delta > \frac{\lambda}{2M_{\text{RF}}}$ , the effective spacing between the  $L$  elements of the virtual antenna formed by the  $L$

subarrays causes the DoA estimates generated by the SPC-MPM approach to be non-unique. In particular, each DoA will result in  $M_{\text{RF}}$  estimates, of which  $M_{\text{RF}} - 1$  are spurious.

*Proof:* From Theorem 2, the spacing between the elements of the virtual antenna array is  $M_{\text{RF}}\Delta$ , causing the phases in the virtual steering vector,  $\psi_{r,\ell} = (\ell - 1)\mu_r M_{\text{RF}}$  in (24), to be multiples of  $M_{\text{RF}}\mu_r$  instead of  $\mu_r$ , as in FD receivers. When  $M_{\text{RF}}\mu_r > 2\pi$ , phase ambiguity arises because phases of the form  $M_{\text{RF}}\mu_r + 2\pi i$ ,  $i \in \mathbb{Z}$ , yield the same virtual steering vector. In other words,  $\tilde{\mu}_i = \mu_r + \frac{2\pi i}{M_{\text{RF}}}$ ,  $\tilde{\mu}_i \in (-\pi, \pi]$ , represents the phase of the  $i$ -th grating lobe, and yields the same virtual steering vector. Hence, there are  $M_{\text{RF}}$  distinct phases associated with  $\mu_r$ , and the set of  $M_{\text{RF}}R$  phases for the  $R$  sources can be expressed as:

$$\mathcal{G} = \left\{ \tilde{\mu}_i \mid \left\lceil \frac{M_{\text{RF}}}{2} \left(-1 - \frac{\mu_r}{\pi}\right) \right\rceil \leq i \leq \left\lfloor \frac{M_{\text{RF}}}{2} \left(1 - \frac{\mu_r}{\pi}\right) \right\rfloor, i \in \mathbb{Z}, \right. \\ \left. r = 1, \dots, R \right\}. \quad (49)$$

We now present a method for resolving the DoA ambiguity elucidated in Corollary 1.

1) *Resolving DoAs Ambiguity:* To address DoA ambiguity, we note that only one of the  $M_{\text{RF}}$  estimated phases for each source corresponds to the true DoA. Such phase can be identified to be the one that maximizes the SNR; a property that is not shared by the remaining  $M_{\text{RF}} - 1$  spurious phases. To this end, we use a set of  $G$  analog combiners,  $\{\mathbf{W}_{A,g}\}_{g=1}^G$ , along with  $G$  segments of snapshots of length  $K$  each. Each element in this set,  $\mathbf{W}_{A,g} \in \mathbb{C}^{M \times L}$ , is constructed as in (10), but with the phases connected to its  $L$  RF chains, i.e., the phases of individual columns, configured using  $L$  distinct phases from  $\mathcal{G}$  in (49). Hence,  $G = \frac{M_{\text{RF}}R}{L} = \frac{MR}{L^2}$ , which, for ease of exposition, will be assumed to be an integer. The  $g$ -th analog combiner,  $\mathbf{W}_{A,g}$ , can be expressed as:

$$\mathbf{W}_{A,g} = \bigoplus_{\ell=1}^L \mathbf{w}_{A,\ell}(\tilde{\mu}_{(g-1)L+\ell}), \quad (50)$$

where, for any  $\beta$ , the  $m$ -th entry of  $\mathbf{w}_{A,\ell}(\beta) \in \mathbb{C}^{M_{\text{RF}} \times 1}$  is  $e^{j(m-1)\beta}$ ,  $m = 1, \dots, M_{\text{RF}}$ , and  $\tilde{\mu}_{(g-1)L+\ell}$  is the  $((g-1)L + \ell)$ -th element of  $\mathcal{G}$  in (49), for  $g = 1, \dots, G$ .

By cycling over the set of analog combiners,  $\{\mathbf{W}_{A,g}\}_{g=1}^G$ , we identify the true  $R$  DoAs as the ones that maximize the SNR at the outputs of the RF chains. In particular, the estimate of true DoA,  $\mu_r$ , corresponds to the phase  $\tilde{\mu}_{j_r^*} \in \mathcal{G}$ , where  $j_r^*$  is the index of the phase that maximizes the SNR of the  $r$ -th source. In other words,

$$j_r^* = \arg \max_{j_r \in \{(r-1)M_{\text{RF}}+1, \dots, rM_{\text{RF}}\}} \frac{\|\mathbf{w}_{A,\ell}^H(\tilde{\mu}_{j_r})\mathbf{A}_\ell \mathbf{S}_g + \mathbf{w}_{A,\ell}^H(\tilde{\mu}_{j_r})\mathbf{Z}_g\|^2}{K\|\mathbf{w}_{A,\ell}(\tilde{\mu}_{j_r})\|^2} - 1, \quad (51)$$

where  $\mathbf{A}_\ell \in \mathbb{C}^{M_{\text{RF}} \times R}$  is the  $\ell$ -th partition of  $\mathbf{A}$ , i.e.,  $\mathbf{A} = [\mathbf{A}_1^T \ \dots \ \mathbf{A}_L^T]^T \in \mathbb{C}^{M \times R}$ . The indices  $g$  and  $\ell$  corresponding to a given  $j_r$  are given by  $g = \lceil \frac{j_r}{L} \rceil$  and  $\ell = j_r - (g-1)L$ . The matrices  $\mathbf{S}_g \in \mathbb{C}^{R \times K}$  and  $\mathbf{Z}_g \in \mathbb{C}^{M \times K}$  are, respectively, the signal and noise components of the  $g$ -th length- $K$  segment of snapshots.

*Remark 4:* Resolving ambiguity requires a small fraction of the total snapshots, e.g.,  $KG = \frac{K}{10}$ , cf. Section V below.  $\square$

*Remark 5:* In SPC-MPM, the vectors  $\{\mathbf{q}_k\}_{k=1}^{\tilde{K}}$ , used to construct the Hankel matrices are  $L$ -dimensional, whereas in FD and PMPM, these vectors are  $M$ -dimensional. The lower dimensionality of SPC-MPM results in reduced resolution, cf. Section V below.  $\square$

*Remark 6:* In FD and PMPM, the number of sources that can be estimated via the MPM is  $R \in [\xi, M - \xi]$ , whereas the corresponding range in SPC-MPM is  $R \in [\xi, L - \xi]$ . These ranges ensure that the rank of the respective Hankel matrices in (12), (31), and (40) is  $R$ .  $\square$

The PMPM and SPC-MPM approaches address the two key challenges in MPM-based DoA estimation: the attenuation imposed by individual analog combiners and the tangling of received signals caused by the HAD architecture. For the first challenge, both approaches mitigate attenuation by cycling over an exhaustive set of analog combiners. For the second challenge, PMPM depends on periodicity to disentangle the received signals. Extracting such periodicity, if exists, requires additional hardware, which may not be available for some receivers. In contrast, SPC-MPM disentangles the output signals of the analog combiner by using single-phase analog combiners. In the next section, numerical results show that both techniques significantly outperform their existing counterparts, especially when the number of snapshots is limited.

## V. SIMULATION

In this section, we compare the RMSE between the actual and the DoA estimates generated by the proposed approaches and the approaches in: 1) root Hybrid Digital Analog Phase Alignment (root-HDAPA) [33], 2) covariance matrix reconstruction (CMR) [34], 3) full spatial coverage and successive refinement (FSCR) [36], and 4) the MPM in FD receivers (FD-MPM) [32]. As a benchmark, the CRLB of the FD [23], [46] and HAD receivers [36] are also depicted. The RMSE is given by  $\sqrt{\frac{1}{RD} \sum_{r=1}^R \sum_{d=1}^D (\theta_r^{(d)} - \hat{\theta}_r^{(d)})^2}$ , where  $D = 2000$  is the number of Monte Carlo trials. For the FD receiver, the  $R \times R$  CRLB matrix is [23], [46]:

$$\text{CRLB}_{\text{FD}}(\boldsymbol{\theta}) = \frac{\sigma_z^2}{2K} \left( \Re \left\{ \mathbf{F}^H \mathbf{P}_A^\perp \mathbf{F} \odot \left( \Phi \mathbf{A}^H \boldsymbol{\Sigma}^{-1} \mathbf{A} \Phi \right)^T \right\} \right)^{-1}, \quad (52)$$

where the  $r$ -th column of  $\mathbf{F} \in \mathbb{C}^{M \times R}$  is  $\mathbf{f}_r = \nabla_{\theta_r} \mathbf{a}(\theta_r)$ ,  $\Phi$  is defined in (5), and  $\boldsymbol{\Sigma} = \mathbb{E}\{\mathbf{X}_n \mathbf{X}_n^H\} = \mathbf{A} \Phi \mathbf{A}^H + \mathbf{I}_M$ .

For SPC-MPM, the analog combiners,  $\{\mathbf{W}_{A,n}\}_{n=1}^N$ , satisfy  $\mathbf{W}_{A,n}^H \mathbf{W}_{A,n} = \frac{M}{L} \mathbf{I}_L$ . Hence, the  $R \times R$  CRLB matrix is [36]:

$$\text{CRLB}_{\text{SPC}}(\boldsymbol{\theta}) = \frac{\sigma_z^2 M}{2KL} \left( \Re \left\{ \sum_{n=1}^N \left( \left( \mathbf{F}^H \mathbf{W}_{A,n} \mathbf{P}_{E_n}^\perp \mathbf{W}_{A,n}^H \mathbf{F} \right) \odot \left( \Phi \mathbf{E}_n^H \boldsymbol{\Upsilon}_n^{-1} \mathbf{E}_n \Phi \right)^T \right) \right\} \right)^{-1}, \quad (53)$$

where  $\mathbf{E}_n = \mathbf{W}_{A,n}^H \mathbf{A}$ , and the  $L \times L$  matrix  $\boldsymbol{\Upsilon}_n = \mathbf{W}_{A,n}^H \mathbf{A} \Phi \mathbf{A}^H \mathbf{W}_{A,n} + \frac{M}{L} \mathbf{I}_L$ ,  $n = 1, \dots, N$ . Using an approach analogous to the one in [36], the CRLB for PMPM can be shown to be given by the FD expression in (52), but with  $K$  snapshots, cf. Theorem 1 in Section IV-A.

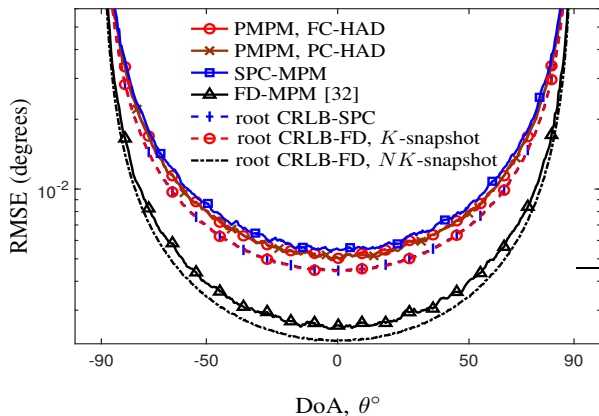


Figure 3: Root CRLBs and RMSEs of proposed approaches.

For fair comparison, the total number of snapshots is set to  $\tilde{K}$  for all receivers. For PMPM and SPC-MPM, the number of analog combiners,  $N = \frac{M}{L}$ . For PMPM, the  $\tilde{K}$  snapshots are used to construct the  $K_A = K = \frac{\tilde{K}}{N}$  Hankel matrices in (32). In contrast, for SPC-MPM,  $\tilde{K}$  is partitioned into  $\tilde{K}_1 + \tilde{K}_2$ , where  $\tilde{K}_1 = K_A$  is used to construct the Hankel matrices in (48), and  $\tilde{K}_2 = \frac{\tilde{K}}{8}$  is used to resolve DoA ambiguity, cf. Section IV-B1, and  $K = \frac{\tilde{K}_1}{N}$ . The matrix pencil parameter is set to  $\xi = \frac{M}{2}$  for PMPM and FD-MPM, and  $\xi = \frac{L}{2}$  for SPC-MPM. The matrix  $\mathcal{S}_n$  in (4) comprising the signals of the  $R$  sources is assumed to be zero-mean Gaussian with independent entries satisfying (5) and  $\mathcal{S}_n = \mathcal{S}$ , for  $n = 1, \dots, N$ . Since  $\sigma_z^2 = 1$ , the receive SNR of the  $r$ -th source is  $P_r$ . The antenna spacing  $\Delta$  in (1b) is set to  $\frac{\lambda}{2}$ .

*Example 1 (Comparison with CRLB):* In this example, we compare the RMSE versus the DoA  $\theta$  for FD-MPM [32] and the approaches proposed herein for HAD receivers when the number of antennas is  $M = 32$ , the number of RF chains is  $L = 8$ , the number of snapshots  $\tilde{K} = 128$ , and the SNR = 20 dB. This comparison is depicted in Figure 3. As a benchmark, we plot the square root of the corresponding root CRLBs. The RMSE of PMPM with FC-HAD and PC-HAD is compared with the root CRLB in (52) with  $K = 32$  snapshots, and that of SPC-MPM is compared with the root CRLB in (53).

From Figure 3, it can be seen that PMPM with FC-HAD and PC-HAD exhibit indistinguishable performance, with a relatively small gap to the root CRLB in (52) with  $K = 32$  snapshots. From Figure 3, it can also be seen that SPC-MPM exhibits a gap to the root CRLB in (53) that is slightly larger than that exhibited by PMPM and its corresponding root CRLB. This gap is mainly due to the snapshots consumed to resolve DoA ambiguity. For instance, at  $\theta = 0^\circ$ , the RMSEs for PMPM with both FC-HAD and PC-HAD are  $0.005^\circ$ , and the corresponding root CRLB is  $0.004^\circ$ , whereas the RMSE for SPC-MPM is  $0.006^\circ$  and its corresponding root CRLB is  $0.004^\circ$ . Finally, it can be seen from Figure 3 that FD-MPM [32] with  $\tilde{K} = 128$  snapshots exhibits a gap to its root CRLB comparable to the corresponding gap between PMPM and SPC-MPM, and their respective root CRLBs.  $\square$

*Example 2 (Verifying Theorems 1 and 2):* In this example, we consider one source with a DoA of  $\theta = 30^\circ$ ,  $M = 64$ ,

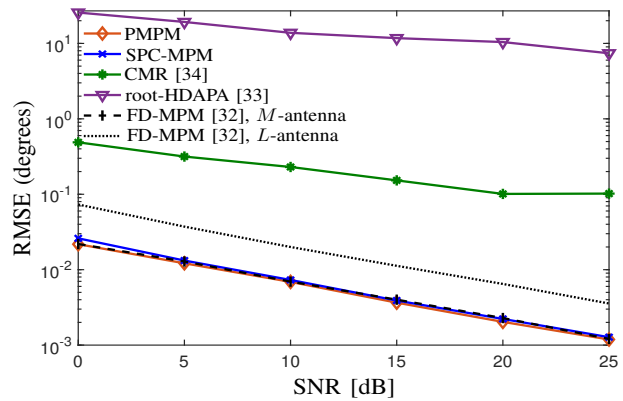


Figure 4: RMSE comparison of proposed approaches.

$L = 8$ ,  $N = 8$  and  $\tilde{K} = 256$ . The RMSE yielded by PMPM, SPC-MPM and that of root-HDAPA [33] and CMR [34] are depicted in Figure 4. For comparison, this figure also shows the RMSE yielded by the FD-MPM [32] in two cases: the first uses  $M$  antennas with  $\Delta = \frac{\lambda}{2}$  and  $K = 32$  snapshots, whereas the second uses  $L$  antennas with  $M_{\text{RF}}\Delta$  spacing and  $K = 28$  snapshots. The respective snapshots for PMPM, CMR, and root-HDAPA are  $\tilde{K}_1 = NK = 256$ . For SPC-MPM,  $\tilde{K}$  is divided into  $\tilde{K}_1 = NK = 224$  and  $\tilde{K}_2 = 32$  snapshots.

From Figure 4, it can be seen that the proposed PMPM and SPC-MPM approaches significantly outperform root-HDAPA [33] and CMR [34]. For instance, at an SNR = 10 dB, the RMSEs yielded by PMPM, and SPC-MPM are  $0.0068^\circ$ , and  $0.0073^\circ$ , respectively. In contrast, the RMSEs for root-HDAPA and CMR are  $13.825^\circ$  and  $0.23^\circ$ , respectively. The performance of root-HDAPA can be attributed to the fixed analog combiner used therein [33], which heavily attenuates signals arriving from particular DoAs. The performance of CMR aligns with the observation made in [34, Section IV] and can be attributed to the, potentially sub-optimal, diagonal loading used in reconstructing the covariance matrix. Figure 4 also shows that PMPM and FD-MPM exhibit identical RMSE performance across all SNRs, coinciding with Theorem 1. For SPC-MPM, we note that, since the DoA of  $\theta = 30^\circ$  coincides with the angle of one of the beams of the  $M_{\text{RF}}$ -DFT matrix, Theorem 2 asserts that the  $M$ -antenna SPC-MPM outperforms the  $L$ -antenna FD-MPM by  $10 \log M_{\text{RF}}$ . Figure 4 verifies this theoretical finding. For instance, at an RMSE of  $0.004^\circ$ , SPC-MPM achieves a 9 dB performance gain over FD-MPM.  $\square$

*Example 3 (Multiple DoA Estimation):* In this example, we compare the RMSE of the proposed approaches with that of FC-FSCR [36]<sup>3</sup> and FD-MPM [32] with four DoAs:  $\theta_1 = -60^\circ$ ,  $\theta_2 = -15^\circ$ ,  $\theta_3 = 35^\circ$ , and  $\theta_4 = 75^\circ$ , when  $M = 64$ ,  $L = 16$ , and  $\tilde{K} = 128$ . The RMSE of all techniques is shown in Figure 5. For FSCR,  $\tilde{K}$  is divided equally between the two underlying algorithms. For the first algorithm, the resolution is set to  $\delta_1 = 10^{-1}$ . For the second algorithm, the number of inner iterations is set to 5, each with  $\nu = 1550$  search steps.

<sup>3</sup>FC-FSCR outperforms PC-FSCR when the number of snapshots is small.

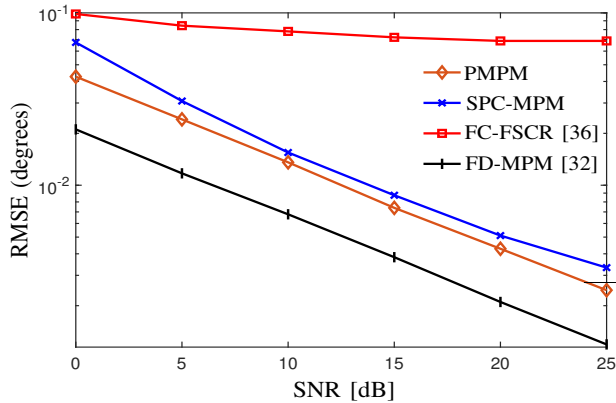


Figure 5: RMSE of proposed approaches for four DoAs.

From Figure 5, it is evident that PMPM outperforms SPC-MPM and FC-FSCR. For instance, at an SNR = 15 dB, the RMSEs of PMPM, SPC-MPM and FC-FSCR are  $0.007^\circ$ ,  $0.009^\circ$  and  $0.07^\circ$ , respectively, while FD-MPM yields an RMSE of  $0.004^\circ$ , which corresponds to a 3 dB gap between the proposed approaches and the FD receiver. The small gap between PMPM and SPC-MPM aligns with the results reported in Example 1. The performance of FC-FSCR is due to the fact that the underlying algorithms rely on statistical averaging [36], which requires a large number of snapshots for accurate estimation. The effect of the number of snapshots on performance will be discussed in Example 5 below.  $\square$

*Example 4 (Resolution):* To assess the resolution of the proposed approaches, we consider  $R = 2$  sources. The DoA of the first source is  $\theta_1 = -15^\circ$ , whereas that of the second source is  $\theta_2 = \theta_1 - \Delta\theta$ , where  $\Delta\theta \in \{0.3^\circ, 0.5^\circ, 2^\circ\}$ . We set  $M = 128$ ,  $L = 16$ ,  $\tilde{K} = 64$ ,  $\tilde{K}_1 = 56$ , and  $\tilde{K}_2 = 8$ .

From Figure 6, it can be seen that the RMSE of all proposed approaches improves monotonically as the angular separation,  $\Delta\theta$ , between the two DoAs increases from  $0.3^\circ$  to  $2^\circ$ . For instance, at an SNR = 10 dB, the RMSE values for PMPM improve from  $0.93^\circ$  to  $0.006^\circ$ , while those for SPC-MPM improve from  $0.36^\circ$  to  $0.007^\circ$  under the same conditions. For  $\Delta\theta = 0.5^\circ$  and  $2^\circ$ , PMPM outperforms SPC-MPM. This can be attributed to the fact that the signal used to construct the Hankel matrix in these techniques is  $M$ -dimensional, whereas that used to construct the Hankel matrix in SPC-MPM is  $L$ -dimensional, cf. Theorems 1 and 2. It can also be seen from Figure 6 that, when  $\Delta\theta$  is reduced to  $0.3^\circ$ , the performance of PMPM is constrained by the SNR until 12 dB, favoring SPC-MPM. For instance, at an RMSE of  $0.4^\circ$ , SPC-MPM offers a 4 dB advantage over PMPM. Beyond that SNR, PMPM outperforms SPC-MPM. For instance, at an RMSE of  $0.02^\circ$ , PMPM offers a 5.7 dB advantage over SPC-MPM.  $\square$

*Example 5 (Effect of Snapshots on Estimation Accuracy):* In this example, we investigate the impact of the number of snapshots on the performance of the proposed approaches and the FC-FSCR technique in [36]. We consider a HAD receiver at an SNR of 10 dB with  $M = 32$ ,  $L = 8$  and a random DoA,  $\theta$  uniformly distributed over  $[-\frac{\pi}{2} + a, \frac{\pi}{2} - a]$ , where  $a = \frac{\pi}{100}$  is chosen to avoid the high estimation error at  $\pm\frac{\pi}{2}$ , cf. Figure 3.

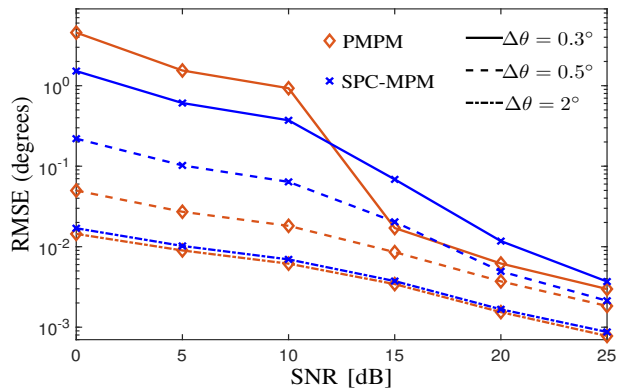


Figure 6: Resolution investigation at  $\Delta\theta = 0.3^\circ, 0.5^\circ, 2^\circ$ .

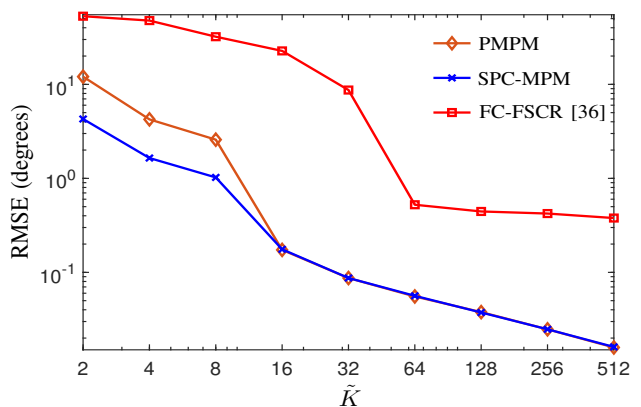


Figure 7: Impact of number of snapshots on RMSE.

For FC-FSCR, we use the same settings as in Example 3. We set  $\tilde{K}_2 = 1$  for  $\tilde{K} < 8$ , and  $\tilde{K}_2 = \frac{\tilde{K}}{8}$  for  $\tilde{K} \geq 8$ .

From Figure 7, it is evident that the RMSE of FC-FSCR is significantly superseded by the proposed approaches. For instance, for  $\tilde{K} = 8$ , the RMSEs for PMPM, SPC-MPM are  $2.6^\circ$ , and  $1^\circ$ , respectively, compared to  $32.1^\circ$  for FC-FSCR. When  $\tilde{K}$  increases to 512, the RMSE of the proposed approaches drops to  $0.016^\circ$ , while FSCR remains at  $0.38^\circ$ . The poor performance of proposed techniques when  $\tilde{K} \leq 3$  is due to the fact that both PMPM and SPC-MPM require a minimum number of snapshots, equal to the number of analog combiners, i.e.,  $\tilde{K} = 4$ . As  $\tilde{K}$  increases, the performance of both PMPM and SPC-MPM continue to improve.  $\square$

## VI. CONCLUSION

We considered the problem of reliable DoA estimation in HAD receivers when the number of snapshots is too small for statistical averaging to be considered accurate. To overcome the difficulties incurred by the small number of snapshots, we invoked matrix pencil constructions. These constructions can be readily used to extract the DoA in FD receivers, but using them in HAD receivers requires several hurdles to be overcome. Towards that end, we developed two approaches. The first approach can be applied in FC-HAD and PC-HAD receivers and exploits the periodicity embedded in the received signals. In contrast, the second approach can be applied to

PC-HAD receivers only, and does not rely on periodicity. Instead, it uses single-phase analog combiners, which results in DoA ambiguity, and requires further processing to be resolved. Numerical simulations show that the proposed approaches exhibit comparable RMSEs, but the first achieves superior resolution at moderate-to-high SNRs. Both approaches significantly outperform their existing counterparts. Comparison with the corresponding CRLBs shows that the performance of the proposed approaches is within a small gap to optimal.

#### APPENDIX A PROOF OF THEOREM 1

We begin by stating the following preliminaries.

*Preliminaries:* Let  $\mathbf{B} \in \mathbb{C}^{M \times M}$  be an arbitrary full rank matrix partitioned as  $\mathbf{B} = [\mathbf{B}_1 \ \cdots \ \mathbf{B}_N]$ . The matrix  $\mathbf{B}_n$  is full column rank, and the projector on its column space is  $\mathbf{P}_{\mathbf{B}_n} = \mathbf{B}_n(\mathbf{B}_n^H \mathbf{B}_n)^{-1} \mathbf{B}_n^H$ . Furthermore,  $\sum_{n=1}^N \mathbf{P}_{\mathbf{B}_n} = \mathbf{I}_M$  and  $\sum_{n \neq m} \mathbf{P}_{\mathbf{B}_n} = \mathbf{P}_{\mathbf{B}_m}^\perp$ , where  $\mathbf{P}_{\mathbf{B}_m}^\perp \in \mathbb{C}^{M \times M}$  is the projector on the null space of  $\mathbf{B}$ .

*Detailed Proof:* The output of the analog combiner,  $\mathbf{W}_{A,n}$ , is given in (8), where  $\mathbf{W}_{A,n}$  is given in (26) for FC-HAD and in (27) for PC-HAD. Setting  $\mathbf{B} = \mathbf{W}_{A,n}$  yields  $\mathbf{P}_{\mathbf{W}_{A,n}} = \frac{1}{\alpha^2 M_{\text{RF}}} \mathbf{W}_{A,n} \mathbf{W}_{A,n}^H$ , where, we have used that  $\mathbf{W}_{A,n}^H \mathbf{W}_{A,n} = \alpha^2 M_{\text{RF}} \mathbf{I}_L$ . In the baseband,  $\mathbf{Q}_n$  in (8) is fed to the  $n$ -th baseband digital combiner,  $\mathbf{W}_{D,n}$ . Our goal is to select  $\mathbf{W}_{D,n}$  to facilitate synthesizing the projector on the column space of  $\mathbf{W}_{A,n}$ . To do so, we set  $\mathbf{W}_{D,n} = \frac{1}{\alpha^2 M_{\text{RF}}} \mathbf{W}_{A,n}^H$ ,  $n = 1, \dots, N$ . Applying this to (8) yields:

$$\mathbf{T}_n = \mathbf{W}_{D,n}^H \mathbf{Q}_n = \mathbf{P}_{\mathbf{W}_{A,n}} \mathbf{A} \mathbf{S}_n + \mathbf{P}_{\mathbf{W}_{A,n}} \mathbf{Z}_n. \quad (54)$$

Aggregating the outputs of the  $N$  digital combiners yields  $\mathbf{Y}_{\text{PMPM}} = \sum_{n=1}^N \mathbf{T}_n$ . This summation cannot be computed because the first term of the summand,  $\mathbf{T}_n$ , contains the unknown signal  $\mathbf{S}_n$ . However, when  $\mathbf{S}_n$  is periodic, i.e.,  $\mathbf{S}_n = \mathbf{S}$ , for  $n = 1, \dots, N$ , we incorporate the identity  $\sum_{n=1}^N \mathbf{P}_{\mathbf{W}_{A,n}} = \mathbf{I}_M$ , to obtain  $\mathbf{Y}_{\text{PMPM}}$  in (29).

Comparing  $\mathbf{Y}_{\text{PMPM}}$  in (29) with the signal corresponding to the  $n$ -th length- $K$  segment in the FD receiver, i.e.,  $\mathbf{X}_n$  in (4), it can be seen that both  $\mathbf{Y}_{\text{PMPM}}$  and  $\mathbf{X}_n$  are  $M \times K$  matrices. However,  $\mathbf{X}_n$  is obtained using  $K$  snapshots, whereas  $\mathbf{Y}_{\text{PMPM}}$  is obtained using  $\tilde{K} = NK$  snapshots. Hence, it can be concluded that  $\mathbf{Y}_{\text{PMPM}} \Big|_{\substack{\tilde{K}=NK \\ \text{SNR}_{\text{PMPM}}}} = \mathbf{X} \Big|_{\substack{\tilde{K}=K \\ \text{SNR}_{\text{FD}}}}$ .

To complete the proof, we note that:

$$\text{SNR}_{\text{FD}} = \frac{\text{Tr}(\mathbf{A} \Phi \mathbf{A}^H)}{M}. \quad (55)$$

It remains to determine  $\text{SNR}_{\text{PMPM}}$ . Towards that end, we have

$$\text{SNR}_{\text{PMPM}} = \frac{\mathbb{E}\{\|\mathbf{A} \mathbf{S}\|_F^2\}}{\mathbb{E}\left\{\left\|\sum_{n=1}^N \mathbf{P}_{\mathbf{W}_{A,n}} \mathbf{Z}_n\right\|_F^2\right\}}. \quad (56)$$

Invoking (5), it can be seen that  $\mathbb{E}\{\|\mathbf{A} \mathbf{S}\|_F^2\} = K \text{Tr}(\mathbf{A} \Phi \mathbf{A}^H)$ . Using the fact that  $\mathbf{P}_{\mathbf{W}_{A,n}}$  is idempotent Hermitian, and  $\sum_{n=1}^N \mathbf{P}_{\mathbf{W}_{A,n}} = \mathbf{I}_M$ , and the fact that:

$$\mathbb{E}\{\mathbf{Z}_n \mathbf{Z}_m^H\} = \begin{cases} K \mathbf{I}_M, & n = m, \\ 0, & n \neq m, \end{cases} \quad (57)$$

we have  $\mathbb{E}\left\{\left\|\sum_{n=1}^N \mathbf{P}_{\mathbf{W}_{A,n}} \mathbf{Z}_n\right\|_F^2\right\} = KM$ , whence

$$\text{SNR}_{\text{PMPM}} = \frac{\text{Tr}(\mathbf{A} \Phi \mathbf{A}^H)}{M}. \quad (58)$$

Combining (55) and (58), concludes the proof.

#### APPENDIX B PROOF OF THEOREM 2

To show the equivalence between the input to the  $L$ -antenna FD receiver and the output of the  $n$ -th analog combiner,  $\mathbf{W}_{\text{APC},n}$ , we compare  $\{x_k[m]\}_{m=1}^M$  in (11) with the signal component of  $\{q_k[\ell]\}_{\ell=1}^L$  in (24). This comparison reveals that they are equivalent but with: i.  $M \leftarrow L$ , ii.  $s_r \leftarrow s_r g(\mu_r - \phi_n)$  and iii.  $e^{j(m-1)\mu_r} \leftarrow e^{j(\ell-1)\mu_r M_{\text{RF}}}$ . The latter assignment and (1b) imply that  $\Delta \leftarrow M_{\text{RF}} \Delta$ .

To see that the number of snapshots needed in the considered PC-HAD architecture is  $NK$  as opposed to the  $K$  snapshots needed for FD receivers, we note from (28) and (1b) with  $\Delta = \frac{\lambda}{2}$ , that the spatial sector covered by the  $n$ -th analog combiner,  $\mathbf{W}_{\text{APC},n}$ , is  $\Theta_n = (\arcsin(\frac{2n-3}{M_{\text{RF}}}), \arcsin(\frac{2n-1}{M_{\text{RF}}})]$  for  $n \in \{1, \dots, \frac{N}{2}\}$ ,  $\Theta_n = (-\frac{\pi}{2}, \arcsin(\frac{2n-1}{M_{\text{RF}}})] \cup (\arcsin(\frac{2n-3}{M_{\text{RF}}}), \frac{\pi}{2})$  for  $n = \frac{N}{2} + 1$  and  $\Theta_n = (\arcsin(\frac{2n-3}{M_{\text{RF}}} - 2), \arcsin(\frac{2n-1}{M_{\text{RF}}} - 2)]$  for  $n \in \{\frac{N}{2} + 2, \dots, N\}$ . As illustrated in Figure 2d, the width of each spatial sector is  $\frac{2\pi}{M_{\text{RF}}}$ . Any DoA lies within the spatial sector defined by  $\mathbf{W}_{\text{APC},n}$ , i.e.,  $\theta_r \in \Theta_n$ , can be estimated, otherwise it will be heavily attenuated or nullified. Thus, using  $\{\mathbf{W}_{\text{APC},n}\}_{n=1}^N$  ensures coverage of all DoAs within  $[-\frac{\pi}{2}, \frac{\pi}{2}]$ . In particular, each  $\mathbf{W}_{\text{APC},n}$  processes the  $n$ -th segment containing  $K$  snapshots,  $n = 1, \dots, N$ . In other words, the projection underlying the PC-HAD receiver requires a total of  $NK$  snapshots to ensure that  $K$  snapshots are received from each DoA. In contrast, such a projection is not part of the FD receiver, and hence, a total of  $K$  snapshots suffices to be received from each DoA. This completes the proof of the first two points of the theorem.

It remains to bound  $\text{SNR}_{\text{SPC},r}$ . Let  $\theta_r$  and  $\mathbf{a}_r$  denote the DoA and the corresponding steering vector (cf. (1a) and (1b)) of the  $r$ -th source, respectively,  $r = 1, \dots, R$ . Let  $\mathbf{a}_{r,\ell} \in \mathbb{C}^{M_{\text{RF}}}$  denote the  $\ell$ -th partition of  $\mathbf{a}_r$ , i.e.,  $\mathbf{a}_r = [\mathbf{a}_{r,1}^T \ \cdots \ \mathbf{a}_{r,L}^T]^T$ . Let  $\theta_r \in \Theta_n$ , then, using (23) and (24), the output SNR for the  $r$ -th source is given by:

$$\text{SNR}_{\text{SPC},r} = P_r \left( \frac{1}{M} \sum_{\ell=1}^L |\mathbf{w}_{\text{APC},\ell}^H \mathbf{a}_{r,1}|^2 \right) \quad (59)$$

$$= \frac{P_r |g(\mu_r - \phi_n)|^2}{M_{\text{RF}}} \leq M_{\text{RF}} P_r, \quad (60)$$

where (59) follows from the fact that  $\mathbf{a}_{r,\ell} = \mathbf{a}_{r,1} e^{j\phi_{r,\ell}}$ . The first part of (60) follows from setting  $\mathbf{w}_{\text{APC},\ell} = \mathbf{v}_n$ , and  $\phi_\ell = \phi_n$  in  $g(\mu_r - \phi_\ell)$ ,  $\forall \ell$ , cf. (25). For the second part of (60), we note that  $\sup_{\mu_r} g(\mu_r - \phi_n) = M_{\text{RF}}$ , and is achieved when  $\mu_r = \phi_n$ , which corresponds to  $\mathbf{a}_{r,\ell} = \mathbf{v}_n$ . The lower bound on  $\text{SNR}_{\text{SPC},r}$  in (39) corresponds to the case in which  $\theta_r$  lies at the edge of  $\Theta_n$ , i.e.,  $\mu_r = \phi_n + \frac{\pi}{M_{\text{RF}}}$ , as illustrated in Figure 2d for  $\mu_r = \phi_1 + \frac{\pi}{4}$ . Substituting  $\mu_r = \phi_n + \frac{\pi}{M_{\text{RF}}}$  into  $g(\mu_r - \phi_n)$  in (25) and (60) yields:

$$\text{SNR}_{\text{SPC},r} = \frac{P_r}{M_{\text{RF}} \sin^2(\frac{\pi}{2M_{\text{RF}}})}. \quad (61)$$

Using (55) in Appendix A, it can be verified that  $\text{SNR}_{\text{FD},r} = P_r$ . Combining (60) and (61), yields (39).

## REFERENCES

- [1] E. Tuncer and B. Friedlander, *Classical and Modern Direction-of-Arrival Estimation*. Amsterdam, Neth.: Academic Press, 2009.
- [2] R. W. Heath, N. Gonzalez-Prelcic, S. Rangan, W. Roh, and A. M. Sayeed, "An overview of signal processing techniques for millimeter wave MIMO systems," *IEEE J. Sel. Topics Signal Process.*, vol. 10, no. 3, pp. 436–453, 2016.
- [3] N. Kaur and S. K. Sood, "An energy-efficient architecture for the Internet of Things (IoT)," *IEEE Syst. J.*, vol. 11, no. 2, pp. 796–805, 2015.
- [4] Z. Fei, B. Li, S. Yang, C. Xing, H. Chen, and L. Hanzo, "A survey of multi-objective optimization in wireless sensor networks: Metrics, algorithms, and open problems," *IEEE Commun. Surv. Tutor.*, vol. 19, no. 1, pp. 550–586, 2016.
- [5] Y. Zeng and R. Zhang, "Energy-efficient UAV communication with trajectory optimization," *IEEE Trans. Commun.*, vol. 16, no. 6, pp. 3747–3760, 2017.
- [6] Y. Wang, C. Li, Y. Huang, D. Wang, T. Ban, and L. Yang, "Energy-efficient optimization for downlink massive MIMO FDD systems with transmit-side channel correlation," *IEEE Trans. Veh. Technol.*, vol. 65, no. 9, pp. 7228–7243, 2015.
- [7] B. Liu, S. Matsushita, and L. Xu, "DOA estimation with small snapshots using weighted mixed norm based on spatial filter," *IEEE Trans. Veh. Technol.*, vol. 69, no. 12, pp. 16183–16187, 2020.
- [8] R. Zhang, B. Shim, and W. Wu, "Direction-of-arrival estimation for large antenna arrays with hybrid analog and digital architectures," *IEEE Trans. Signal Process.*, vol. 70, pp. 72–88, 2021.
- [9] X. Zhang, A. F. Molisch, and S.-Y. Kung, "Variable-phase-shift-based RF-baseband codesign for MIMO antenna selection," *IEEE Trans. Signal Process.*, vol. 53, no. 11, pp. 4091–4103, 2005.
- [10] Q. Shi, M. Razaviyayn, Z.-Q. Luo, and C. He, "An iteratively weighted MMSE approach to distributed sum-utility maximization for a MIMO interfering broadcast channel," *IEEE Trans. Signal Process.*, vol. 59, no. 9, pp. 4331–4340, 2011.
- [11] C. H. Doan, S. Emami, D. A. Sobel, A. M. Niknejad, and R. W. Brodersen, "Design considerations for 60 GHz CMOS radios," *IEEE Commun. Mag.*, vol. 42, no. 12, pp. 132–140, 2004.
- [12] W. Roh, J.-Y. Seol, J. Park, B. Lee, J. Lee, Y. Kim, J. Cho, K. Cheun, and F. Aryanfar, "Millimeter-wave beamforming as an enabling technology for 5G cellular communications: Theoretical feasibility and prototype results," *IEEE Commun. Mag.*, vol. 52, no. 2, pp. 106–113, 2014.
- [13] S. Han, I. Chih-Lin, Z. Xu, and C. Rowell, "Large-scale antenna systems with hybrid analog and digital beamforming for millimeter wave 5G," *IEEE Commun. Mag.*, vol. 53, no. 1, pp. 186–194, 2015.
- [14] A. Alkhateeb, O. El Ayach, G. Leus, and R. W. Heath, "Channel estimation and hybrid precoding for millimeter wave cellular systems," *IEEE J. Sel. Topics Signal Process.*, vol. 8, no. 5, pp. 831–846, 2014.
- [15] O. El Ayach, S. Rajagopal, S. Abu-Surra, Z. Pi, and R. W. Heath, "Spatially sparse precoding in millimeter wave MIMO systems," *IEEE Trans. Commun.*, vol. 13, no. 3, pp. 1499–1513, 2014.
- [16] F. Sotiriou and W. Yu, "Hybrid digital and analog beamforming design for large-scale antenna arrays," *IEEE J. Sel. Topics Signal Process.*, vol. 10, no. 3, pp. 501–513, 2016.
- [17] J. Du, W. Xu, H. Shen, X. Dong, and C. Zhao, "Hybrid precoding architecture for massive multiuser MIMO with dissipation: Sub-connected or fully connected structures?," *IEEE Trans. Wireless Commun.*, vol. 17, no. 8, pp. 5465–5479, 2018.
- [18] X. Yu, J.-C. Shen, J. Zhang, and K. B. Letaief, "Alternating minimization algorithms for hybrid precoding in millimeter wave MIMO systems," *IEEE J. Sel. Topics Signal Process.*, vol. 10, no. 3, pp. 485–500, 2016.
- [19] R. Méndez-Rial, C. Rusu, N. González-Prelcic, A. Alkhateeb, and R. W. Heath, "Hybrid MIMO architectures for millimeter wave communications: Phase shifters or switches?," *IEEE Access*, vol. 4, pp. 247–267, 2016.
- [20] X. Gao, L. Dai, S. Han, I. Chih-Lin, and R. W. Heath, "Energy-efficient hybrid analog and digital precoding for mmWave MIMO systems with large antenna arrays," *IEEE J. Sel. Areas Commun.*, vol. 34, no. 4, pp. 998–1009, 2016.
- [21] H. Krim and M. Viberg, "Two decades of array signal processing research: the parametric approach," *IEEE Signal Process. Mag.*, vol. 13, no. 4, pp. 67–94, 1996.
- [22] J. Capon, "Maximum-likelihood spectral estimation," *Nonlinear methods of spectral analysis*, pp. 155–179, 2005.
- [23] P. Stoica and A. Nehorai, "MUSIC, maximum likelihood, and Cramer-Rao bound," *IEEE Trans. Acoust., Speech, Signal Process.*, vol. 37, no. 5, pp. 720–741, 1989.
- [24] R. Kumaresan and D. W. Tufts, "Estimating the angles of arrival of multiple plane waves," *IEEE Trans. Aerosp. Electron. Syst.*, no. 1, pp. 134–139, 1983.
- [25] R. Schmidt, "Multiple emitter location and signal parameter estimation," *IEEE Trans. Antennas Propag.*, vol. 34, no. 3, pp. 276–280, 1986.
- [26] A. Barabell, "Improving the resolution performance of eigenstructure-based direction-finding algorithms," in *Proc. IEEE Int. Conf. Acoust., Speech, Signal Process.*, vol. 8, pp. 336–339, IEEE, 1983.
- [27] R. Roy and T. Kailath, "ESPRIT-estimation of signal parameters via rotational invariance techniques," *IEEE Trans. Acoust., Speech, Signal Process.*, vol. 37, no. 7, pp. 984–995, 1989.
- [28] N. Yilmazer, J. Koh, and T. K. Sarkar, "Utilization of a unitary transform for efficient computation in the matrix pencil method to find the direction of arrival," *IEEE Trans. Antennas Propag.*, vol. 54, no. 1, pp. 175–181, 2006.
- [29] T. K. Sarkar and O. Pereira, "Using the matrix pencil method to estimate the parameters of a sum of complex exponentials," *IEEE Antennas Propag. Mag.*, vol. 37, no. 1, pp. 48–55, 1995.
- [30] A. Gaber and A. Omar, "A study of wireless indoor positioning based on joint TDOA and DOA estimation using 2-D matrix pencil algorithms and IEEE 802.11 ac," *IEEE Trans. Wireless Commun.*, vol. 14, no. 5, pp. 2440–2454, 2014.
- [31] Y. Hua and T. K. Sarkar, "Matrix pencil method for estimating parameters of exponentially damped/undamped sinusoids in noise," *IEEE Trans. Acoust., Speech, Signal Process.*, vol. 38, no. 5, pp. 814–824, 1990.
- [32] N. Yilmazer, S. Ari, and T. K. Sarkar, "Multiple snapshot direct data domain approach and ESPRIT method for direction of arrival estimation," *Digit. Signal Process.*, vol. 18, no. 4, pp. 561–567, 2008.
- [33] F. Shu, Y. Qin, T. Liu, L. Gui, Y. Zhang, J. Li, and Z. Han, "Low-complexity and high-resolution DOA estimation for hybrid analog and digital massive MIMO receive array," *IEEE Trans. Commun.*, vol. 66, no. 6, pp. 2487–2501, 2018.
- [34] S. Li, Y. Liu, L. You, W. Wang, H. Duan, and X. Li, "Covariance matrix reconstruction for DOA estimation in hybrid massive MIMO systems," *IEEE Wireless Commun. Lett.*, vol. 9, no. 8, pp. 1196–1200, 2020.
- [35] Z. Guo, X. Wang, and W. Heng, "Millimeter-wave channel estimation based on 2-D beamspace MUSIC method," *IEEE Trans. Wireless Commun.*, vol. 16, no. 8, pp. 5384–5394, 2017.
- [36] A. Abdelbadi, M. Mostafa, S. Bameri, R. H. Gohary, and D. Thomas, "DoA estimation for hybrid receivers: Full spatial coverage and successive refinement," *IEEE Trans. Signal Process.*, vol. 72, pp. 4730–4744, 2024.
- [37] M. M. Mulu, P. Xiao, M. Khalily, K. Cumanan, L. Zhang, and R. Tafazolli, "Low-complexity and robust hybrid beamforming design for multi-antenna communication systems," *IEEE Trans. Wireless Commun.*, vol. 17, no. 3, pp. 1445–1459, 2017.
- [38] H. Huang, J. Yang, H. Huang, Y. Song, and G. Gui, "Deep learning for super-resolution channel estimation and DOA estimation based massive MIMO system," *IEEE Trans. Veh. Technol.*, vol. 67, no. 9, pp. 8549–8560, 2018.
- [39] Z.-M. Liu, C. Zhang, and S. Y. Philip, "Direction-of-arrival estimation based on deep neural networks with robustness to array imperfections," *IEEE Trans. Antennas Propag.*, vol. 66, no. 12, pp. 7315–7327, 2018.
- [40] A. M. Elbir, K. V. Mishra, M. B. Shankar, and B. Ottersten, "A family of deep learning architectures for channel estimation and hybrid beamforming in multi-carrier mm-wave massive MIMO," *IEEE Trans. Cogn. Commun. Netw.*, 2021.
- [41] D. Tse and P. Viswanath, *Fundamentals of Wireless Communication*. Cambridge, U.K.: Cambridge Univ. Press, 2005.
- [42] G. H. Golub and C. F. V. Loan, *Matrix Computations*. Baltimore, MD, USA: JHU Press, 2013.
- [43] M. A. Swillam, R. H. Gohary, M. H. Bakr, and X. Li, "Efficient approach for sensitivity analysis of lossy and leaky structures using FDTD," *Prog. Electromagn. Res.*, vol. 94, pp. 197–212, 2009.
- [44] G. Boutry, M. Elad, G. H. Golub, and P. Milanfar, "The generalized eigenvalue problem for nonsquare pencils using a minimal perturbation approach," *SIAM J. Matrix Anal. Appl.*, vol. 27, no. 2, pp. 582–601, 2005.
- [45] Y. Hua and T. Sarkar, "On SVD for estimating generalized eigenvalues of singular matrix pencil in noise," *IEEE Trans. Signal Process.*, vol. 39, no. 4, pp. 892–900, 1991.
- [46] P. Stoica and A. Nehorai, "Performance study of conditional and unconditional direction-of-arrival estimation," *IEEE Trans. Acoust., Speech, Signal Process.*, vol. 38, no. 10, pp. 1783–1795, 1990.